19

THE FINITE ELEMENT METHOD

19.1

INTRODUCTION

The finite element method* is the most powerful numerical technique available today for the analysis of complex structural and mechanical systems. It is used to obtain numerical solutions to a wide range of problems. The finite element method is used to analyze both linear and nonlinear systems. Nonlinear analysis includes material yielding, creep or cracking; aeroelastic response; buckling and postbuckling response; contact and friction; etc. The finite element method is used for both static and dynamic analyses. In its most general form, the method is not restricted to structural (or mechanical) systems. It has been applied to problems in fluid flow, heat transfer, and electric potential. This versatility is a major reason for the popularity of the method.

A complete study of finite element methods is beyond the scope of this book. So, the objective of this chapter is to outline the basic formulation for problems in linear elasticity. The formulation for plane elasticity is presented first. Then, the use of the method to analyze framed structures is examined. Finally, accuracy, convergence, and modeling techniques are discussed. Advanced topics, such as analysis of plate bending and shell problems, three-dimensional problems, and dynamic and nonlinear analysis, are left to more specialized texts.

Analytical Perspective

The classical method of analysis in elasticity involves the study of an infinitesimal element of an elastic body (continuum or domain). Relationships among stress, strain, and displacement for the infinitesimal element are developed (see Chapters 1–3) that are usually in the form of differential (or integral) equations that apply to each point in the body. These equations must be solved subject to appropriate boundary conditions. In other words, the approach is to define and solve a classical boundary value problem in mathematics (Boresi and Chong, 1987). Problems in engineering usually involve very complex shapes and boundary conditions. Consequently, for such cases, the equations cannot be solved exactly, but must finally be solved by approximate methods; for example, by truncated series, finite differences,

* The discovery of the method is often attributed to Courant (1943). The use of the method in structural (aircraft) analysis was first reported by Turner et al. (1956). The method received its name from Clough (1960).

numerical integration, etc. All these approximate methods require some form of discretization of the solution.

By contrast, the formulation of finite element solutions recognizes at the outset that discretization is likely to be required. The first step in application of the method is to discretize the domain into an assemblage of a finite number of finite size *elements* (or subregions) that are connected at specified node points. The quantities of interest (usually nodal displacements) are assumed to vary in a particular fashion over the element. This *assumed* element behavior leads to relatively simple integral equations for the individual elements. The integral equations for an element are evaluated to produce algebraic equations (in the case of static loading) in terms of the displacements of the node points. The algebraic equations for all elements are assembled to achieve a system of equations for the structure as a whole. Appropriate numerical methods are then used to solve this system of equations.

In summary, using the classical approach, we often are confronted with differential (or integral) equations that cannot be solved in closed form. This is due to the complexity of the geometry of the domain or boundary conditions. Consequently, we are forced to use numerical methods to obtain an approximate solution. These numerical methods always involve some type of discretization. In the finite element method, the discretization is performed at the outset. Then, further approximations, either in the formulation or in the solution may not be necessary.

Sources of Error

There are three sources of error in the finite element method: errors due to approximation of the domain (discretization error), errors due to approximation of the element behavior (formulation error), and errors due to use of finite precision arithmetic (numerical error).

Discretization error is due to the approximation of the domain with a finite number of elements of fixed geometry. For instance, consider the analysis of a rectangular plate with a centrally located hole (Fig. 19.1*a*). Due to symmetry, it is sufficient to model only one-quarter of the plate. If the region is subdivided into triangular elements (a triangular mesh or grid), the circular hole is approximated by a series of straight lines. If a few large triangles are used in a coarse mesh, (Fig. 19.1*b*), greater discretization error results than if a large number of small elements are used in a fine mesh, (Fig. 19.1*c*). Other geometric shapes may be chosen for the elements. For example, with quadrilateral elements that can represent curved sides, the circular hole is more accurately approximated (Fig. 19.1*d*). Hence, discretization error may be reduced by grid refinement. The grid can be refined by using more elements of the same type but of smaller size (*h-refinement*, Cook et al., 1989) or by using elements of a different type (*p-refinement*).

Formulation error results from the use of finite elements that do not precisely describe the behavior of the continuum. For instance, a particular element might be formulated on the assumption that displacements vary linearly over the domain. Such an element would contain no formulation error when used to model a prismatic bar under constant tensile load; in this case, the assumed displacement matches the actual displacement. If the same bar were subjected to uniformly distributed body force, then the actual displacements vary quadratically and formulation error would exist. Formulation error can be minimized by proper selection of element type and appropriate grid refinement.

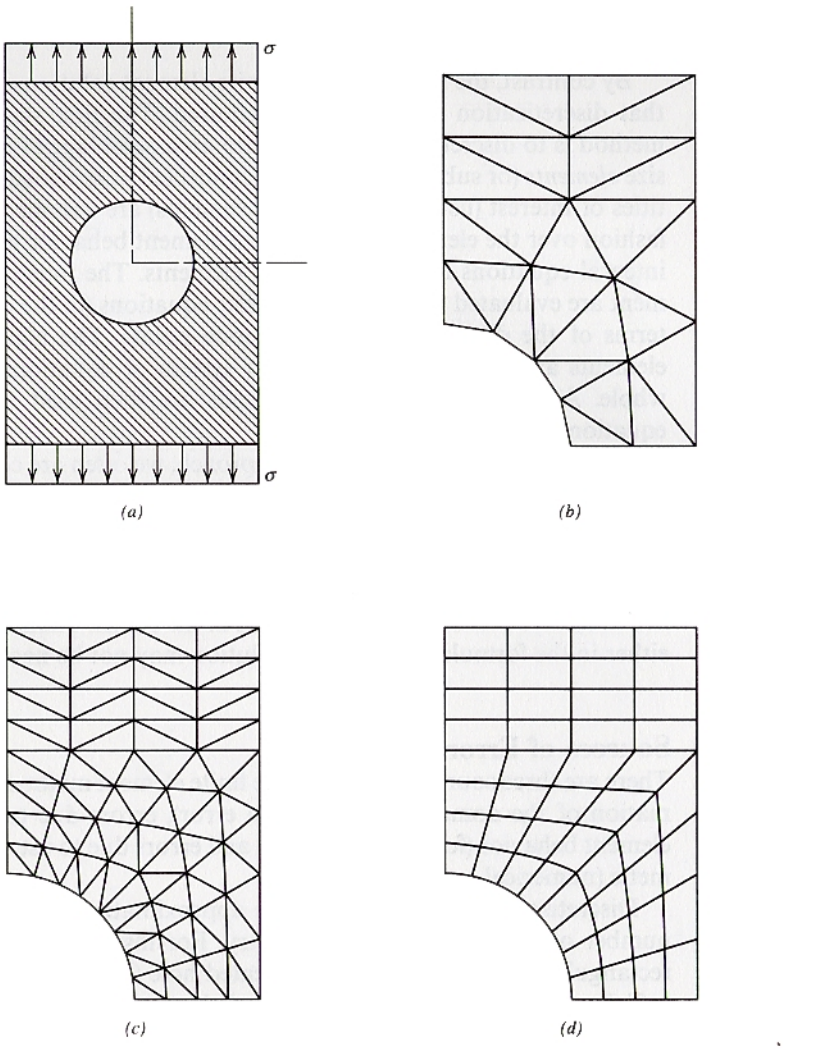

Figure 19.1 Finite element models of plate with centrally located hole. (*a*) Plate geometry and loading. (*b*) Coarse mesh of triangles. (*c*) Fine mesh of triangles. (*d*) Mesh of quadrilaterals with curved edges.

Numerical error is a consequence of round-off during floating-point computations and the error associated with numerical integration procedures. This source of error is dependent on the order in which computations are performed in the program and the use of double or extended precision variables and functions. The use of bandwidth minimization* can help control numerical error. Generally, in a well-designed finite element program, numerical error is small relative to formulation error.

* See Sec. 19.6 for a discussion of bandwidth minimization.

19.2

FORMULATION FOR PLANE ELASTICITY

Elasticity Concepts

One approach for developing the algebraic equations of the finite element method is to use energy principles. Fundamental energy expressions for an elastic solid are presented in Chapters 3 and 5. For plane elasticity, these expressions are simplified appropriately. The first law of thermodynamics states that for a two-dimensional body in equilibrium and subjected to arbitrary virtual displacements $(\delta u, \delta v)$, the variation in work of the external forces δW is equal to the variation of internal energy δU. Since *virtual displacements* are imposed, we define δW as the *virtual work of the external loads* and δU as the *virtual work of the internal forces.* The virtual work of the external loads δW can be divided into the work δW_S of the surface tractions, the work δW_B of the body forces, and the work δW_C* of the concentrated forces. For a two-dimensional body, these quantities are [see Eqs. (3.1a), (3.3), (3.4), (3.7) and (3.8) for definitions of the terms used]

$$\delta W - \delta U = \delta W_S + \delta W_B + \delta W_C - \delta U = 0 \tag{19.1}$$

$$\delta W_S = \int_S (\sigma_{Px}\,\delta u + \sigma_{Py}\,\delta v)\,dS \tag{19.2}$$

$$\delta W_B = \int_V (B_x\,\delta u + B_y\,\delta v)\,dV \tag{19.3}$$

$$\delta W_C = \sum F_{ix}\,\delta u_i + \sum F_{iy}\,\delta v_i \tag{19.4}$$

$$\delta U = \int_V (\sigma_{xx}\,\delta\epsilon_{xx} + \sigma_{yy}\,\delta\epsilon_{yy} + \sigma_{xy}\,\delta\gamma_{xy})\,dV \tag{19.5}$$

where (F_{ix}, F_{iy}) are (x, y) components of the concentrated force F_i at point i, $(\delta u_i, \delta v_i)$ are (x, y) components of the virtual displacement at point i, and $\gamma_{xy} = 2\epsilon_{xy}$. In matrix† notation,

$$\delta W_S = \int_S \{\delta u\}^T \{F_S\}\,dS \tag{19.6}$$

$$\delta W_B = \int_V \{\delta u\}^T \{F_B\}\,dV \tag{19.7}$$

$$\delta W_C = \sum \{\delta u_i\}^T \{F_i\} \tag{19.8}$$

$$\delta U = \int_V \{\delta\epsilon\}^T \{\sigma\}\,dV \tag{19.9}$$

* Concentrated forces were not discussed in Chapter 3 or 5, but are included here for completeness.

† In this chapter, vector quantities are denoted with braces { }. Two-dimensional arrays are contained in brackets [ ].

where

$$\{\delta u\} = [\delta u \quad \delta v]^T$$
$$\{\delta u_i\} = [\delta u_i \quad \delta v_i]^T$$
$$\{F_S\} = [\sigma_{Px} \quad \sigma_{Py}]^T$$
$$\{F_B\} = [B_x \quad B_y]^T$$
$$\{F_i\} = [F_{ix} \quad F_{iy}]^T$$
$$\{\delta\epsilon\} = [\delta\epsilon_{xx} \quad \delta\epsilon_{yy} \quad \delta\gamma_{xy}]^T$$
$$\{\sigma\} = [\sigma_{xx} \quad \sigma_{yy} \quad \sigma_{xy}]^T$$

In matrix form, the two-dimensional linear-elastic stress-strain relations are, by appropriate simplification of Eq. (3.32),

$$\{\sigma\} = [D]\{\epsilon\} \tag{19.10}$$

where $\{\epsilon\} = \{\epsilon_{xx} \quad \epsilon_{yy} \quad \gamma_{xy}]^T$ and $[D]$ is the matrix of elastic coefficients. For plane stress,

$$[D] = \frac{E}{1-\nu^2}\begin{bmatrix} 1 & \nu & 0 \\ \nu & 1 & 0 \\ 0 & 0 & \dfrac{1-\nu}{2} \end{bmatrix} \tag{19.11}$$

and for plane strain,

$$[D] = \frac{E}{(1+\nu)(1-2\nu)}\begin{bmatrix} 1-\nu & \nu & 0 \\ \nu & 1-\nu & 0 \\ 0 & 0 & \dfrac{1-2\nu}{2} \end{bmatrix} \tag{19.12}$$

Similarly, the two-dimensional, small displacement, strain-displacement relations are [see Eq. (2.81)],

$$\{\epsilon\} = [L]\{u\} \tag{19.13}$$

where $\{u\} = [u(x,y) \quad v(x,y)]^T$ and $[L]$ is a matrix of linear differential operators

$$[L] = \begin{bmatrix} \dfrac{\partial}{\partial x} & 0 \\ 0 & \dfrac{\partial}{\partial y} \\ \dfrac{\partial}{\partial y} & \dfrac{\partial}{\partial x} \end{bmatrix} \tag{19.14}$$

Displacement Interpolation: The Constant Strain Triangle

Consider a plane elasticity problem such as that shown in Fig. 19.1*a*. As discussed above, the first step in applying the finite element method is the discretization of

the domain into a finite number of elements. Consider triangular elements as shown in Figs. 19.1*b* and *c*. If the entire domain is in equilibrium, then too is each element. Hence, the above virtual work concepts can be applied to an individual triangular element.

A typical triangular element is shown in Fig. 19.2 with corner nodes 1, 2, and 3 numbered in a counterclockwise order. The (x, y) displacement components at the nodes are (u_1, v_1), (u_2, v_2), and (u_3, v_3) as shown. The *nodal* displacements are the primary variables (unknowns) that are to be determined in the analysis. In general, for plane elasticity elements, node i has two degrees of freedom (DOF), u_i and v_i, where the subscript identifies the node at which the DOF exist. Quantities that are continuous over the element (those not associated with a particular node) are denoted without a subscript. A single triangular element with three nodes has six nodal DOF. These DOF are ordered according to node numbering as

$$\{u_i\} = [u_1 \quad v_1 \quad u_2 \quad v_2 \quad u_3 \quad v_3]^T \tag{19.15}$$

Displacements (u, v) at any point P within the element are continuous functions of the spatial coordinates (x, y). A fundamental approximation in the finite element method (that leads to formulation error) is that the displacement (u, v) at any point P in the element can be written in terms of the nodal displacements. Specifically, the displacement (u, v) at point P within the element is *interpolated* from the displacements of the nodes using interpolation polynomials. The order of the interpolation depends on the number of DOF in the element. For the three-node triangular element, the displacement is assumed to vary linearly over the element.

$$\begin{aligned} u(x, y) &= a_1 + a_2 x + a_3 y \\ v(x, y) &= a_4 + a_5 x + a_6 y \end{aligned} \tag{19.16}$$

The coefficients a_i are constants (sometimes called generalized displacement coordinates) that are evaluated in terms of the nodal displacements. Before making this evaluation, we consider some properties of the linear displacement approximation.

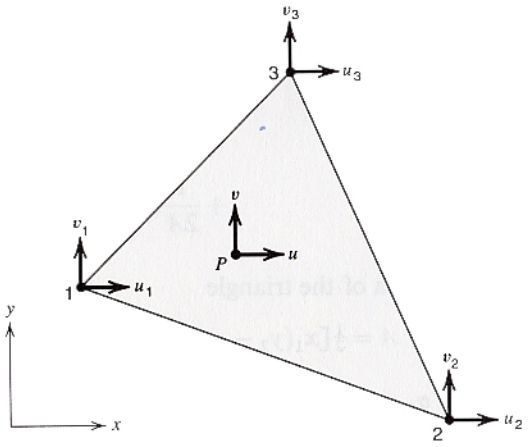

Figure 19.2 Constant strain triangle element.

1. Substitution of Eq. (19.16) into Eq. (19.13) yields $\epsilon_{xx} = a_2$, $\epsilon_{yy} = a_6$, and $\gamma_{xy} = a_3 + a_5$. Thus, the strain components in the element are constant; hence, the name *constant strain triangle* (CST) element. Since the stress-strain relations are linear [Eq. (19.10)], stress components are also constant in the element.
2. If $a_2 = a_3 = a_5 = a_6 = 0$, then $u(x, y) = a_1$ and $v(x, y) = a_4$. Constant values of u and v displacement indicate that the element can represent rigid-body translation.
3. If $a_1 = a_2 = a_4 = a_6 = 0$ and $a_3 = -a_5$, then $u(x, y) = a_3 y$ and $v(x, y) = -a_3 x$. Thus, for small strains and small rotations, the element can represent rigid-body rotation.

These three element characteristics ensure that the solution will converge monotonically as the mesh is refined (see Sec. 19.6 for a discussion of convergence).

To express the continuous displacement field in terms of the nodal displacements, Eq. (19.16) is evaluated at each node. The resulting equations are then solved for the coefficients a_i. Consider first the u displacement.

$$\begin{aligned} u(x_1, y_1) &= a_1 + a_2 x_1 + a_3 y_1 = u_1 \\ u(x_2, y_2) &= a_1 + a_2 x_2 + a_3 y_2 = u_2 \\ u(x_3, y_3) &= a_1 + a_2 x_3 + a_3 y_3 = u_3 \end{aligned}$$

In matrix form, these equations are written as

$$[A]\{a\} = \{u_i\} \tag{19.17}$$

where

$$[A] = \begin{bmatrix} 1 & x_1 & y_1 \\ 1 & x_2 & y_2 \\ 1 & x_3 & y_3 \end{bmatrix}, \qquad \{a\} = \begin{Bmatrix} a_1 \\ a_2 \\ a_3 \end{Bmatrix}, \qquad \text{and} \qquad \{u_i\} = \begin{Bmatrix} u_1 \\ u_2 \\ u_3 \end{Bmatrix}$$

Solution of Eq. (19.17) for $\{a\}$ and substitution into Eq. (19.16) yields

$$\begin{aligned} u(x, y) = {} & \frac{1}{2A}(\alpha_1 + \beta_1 x + \gamma_1 y)u_1 \\ & + \frac{1}{2A}(\alpha_2 + \beta_2 x + \gamma_2 y)u_2 \\ & + \frac{1}{2A}(\alpha_3 + \beta_3 x + \gamma_3 y)u_3 \end{aligned} \tag{19.18}$$

where A is the area of the triangle

$$A = \tfrac{1}{2}[x_1(y_2 - y_3) + x_2(y_3 - y_1) + x_3(y_1 - y_2)] \tag{19.19}$$

and

$$\begin{aligned} \alpha_1 &= x_2 y_3 - x_3 y_2, & \beta_1 &= y_2 - y_3, & \gamma_1 &= x_3 - x_2 \\ \alpha_2 &= x_3 y_1 - x_1 y_3, & \beta_2 &= y_3 - y_1, & \gamma_2 &= x_1 - x_3 \\ \alpha_3 &= x_1 y_2 - x_2 y_1, & \beta_3 &= y_1 - y_2, & \gamma_3 &= x_2 - x_1 \end{aligned} \tag{19.20}$$

Similarly, for the v displacement,

$$v(x,y) = \frac{1}{2A}(\alpha_1 + \beta_1 x + \gamma_1 y)v_1 + \frac{1}{2A}(\alpha_2 + \beta_2 x + \gamma_2 y)v_2 + \frac{1}{2A}(\alpha_3 + \beta_3 x + \gamma_3 y)v_3 \tag{19.21}$$

The functions that multiply the nodal displacements in Eqs. (19.18) and (19.21) are known as *shape* functions (other common names are *interpolation* and *basis* functions). The shape functions for the CST element are

$$N_1(x,y) = \frac{1}{2A}(\alpha_1 + \beta_1 x + \gamma_1 y)$$

$$N_2(x,y) = \frac{1}{2A}(\alpha_2 + \beta_2 x + \gamma_2 y)$$

$$N_3(x,y) = \frac{1}{2A}(\alpha_3 + \beta_3 x + \gamma_3 y) \tag{19.22}$$

Then Eqs. (19.18) and (19.21) take the form

$$u(x,y) = \sum_{i=1}^{3} N_i u_i, \qquad v(x,y) = \sum_{i=1}^{3} N_i v_i$$

In matrix notation

$$\{u\} = [N]\{u_i\} \tag{19.23}$$

where

$$\{u\} = [u(x,y) \quad v(x,y)]^T$$

$$[N] = \begin{bmatrix} N_1 & 0 & N_2 & 0 & N_3 & 0 \\ 0 & N_1 & 0 & N_2 & 0 & N_3 \end{bmatrix} \tag{19.24}$$

The shape functions for the CST element are illustrated in Fig. 19.3, where $N_1 = 1$ at node 1 and $N_1 = 0$ at nodes 2 and 3. Shape functions N_2 and N_3 behave similarly. Another important characteristic of the shape functions is that

$$\sum_{i=1}^{3} N_i(x,y) = 1.0$$

which is a requirement for shape functions so that the element can represent rigid-body motion.

Element Stiffness Matrix: The Constant Strain Triangle

With the displacement field for the element expressed in terms of the nodal displacements, the remainder of the formulation involves relatively straightforward

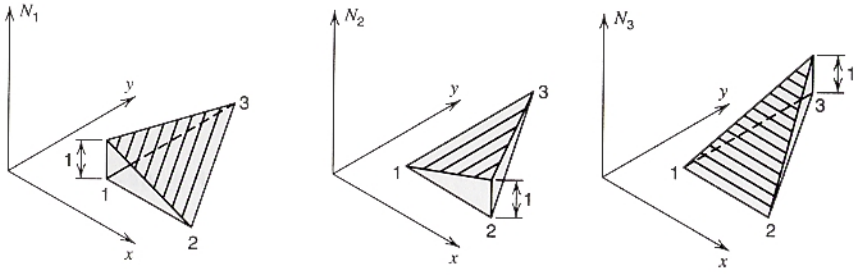

Figure 19.3 Graphical representation of shape functions for the CST element.

manipulation of the virtual work expressions [Eqs. (19.1), (19.6–19.9)]. Consider first the strain-displacement relations. Substitution of Eq. (19.23) into Eq. (19.13) gives the relationship between *continuous* element strains and *nodal* displacements

$$\{\epsilon\} = [L][N]\{u_i\} = [B]\{u_i\} \tag{19.25}$$

where, by Eqs. (19.14) and (19.24),

$$[B] = \left[\begin{array}{cc|cc|cc} \dfrac{\partial N_1}{\partial x} & 0 & \dfrac{\partial N_2}{\partial x} & 0 & \dfrac{\partial N_3}{\partial x} & 0 \\ 0 & \dfrac{\partial N_1}{\partial y} & 0 & \dfrac{\partial N_2}{\partial y} & 0 & \dfrac{\partial N_3}{\partial y} \\ \dfrac{\partial N_1}{\partial y} & \dfrac{\partial N_1}{\partial x} & \dfrac{\partial N_2}{\partial y} & \dfrac{\partial N_2}{\partial x} & \dfrac{\partial N_3}{\partial y} & \dfrac{\partial N_3}{\partial x} \end{array}\right] \tag{19.26}$$

where $[B]$ is partitioned into nodal submatrices. The matrix $[B]$ is sometimes called the semidiscretized gradient operator. Since the shape functions for the CST element are linear in x and y, $[B]$ contains only constants that depend on the nodal coordinates.

For simplicity, temporarily assume that no body forces or surface tractions are applied to the element. However, concentrated loads at node points are permitted. The virtual work of these loads is [see Eq. (19.8)]

$$\delta W = \delta W_C = \{\delta u_i\}^T\{F_i\} \tag{19.27}$$

Substitution of Eqs. (19.27) and (19.9) into (19.1) leads to

$$\{\delta u_i\}^T\{F_i\} - \int_V \{\delta\epsilon\}^T\{\sigma\}\, dV = 0 \tag{19.28}$$

Note that $\{\sigma\} = [D]\{\epsilon\}$, $\{\epsilon\} = [B]\{u_i\}$, and $\{\delta\epsilon\}^T = \{\delta u_i\}^T[B]^T$. Substitution of these expressions into Eq. (19.28) gives

$$\{\delta u_i\}^T\{F_i\} - \int_V \{\delta u_i\}^T[B]^T[D][B]\{u_i\}\, dV = 0$$

Since $\{u_i\}$ and $\{\delta u_i\}$ are *nodal* quantities, they can be removed from the integral. Thus,

$$\{\delta u_i\}^T\left(\{F_i\} - \left[\int_V [B]^T[D][B]\,dV\right]\{u_i\}\right) = 0 \tag{19.29}$$

Since $\{\delta u_i\}$ is arbitrary, Eq. (19.29) yields the result

$$\{F_i\} = \left[\int_V [B]^T[D][B]\,dV\right]\{u_i\}$$

or

$$\{F_i\} = [K]\{u_i\} \tag{19.30}$$

where

$$[K] = \int_V [B]^T[D][B]\,dV \tag{19.31}$$

The element stiffness matrix $[K]$ relates nodal loads to nodal displacements in a system of linear algebraic equations; see Eq. (19.30). For the CST element, all terms in the integral are constants. Hence, for an element of constant thickness t and area A, the element stiffness matrix is

$$[K] = At[B]^T[D][B] \tag{19.32}$$

The individual terms in $[K]$ are denoted k_{ij}, where $i, j = 1, 2, \ldots, 6$ are the row and column positions, respectively. Since the element has six nodal DOF, $[K]$ has order (6×6). The explicit form of the CST element siffness matrix for a plane stress condition is given in Table 19.1.

Examination of Eq. (19.30) helps to establish a physical interpretation of the stiffness coefficients (the individual terms in $[K]$). Let a unit displacement be assigned to u_1 and take all other DOF to be zero. The resulting displacement vector is

$$\{u_i\} = [1 \quad 0 \quad 0 \quad 0 \quad 0 \quad 0]^T$$

Substitution of this displacement vector into Eq. (19.30) gives the force vector required to maintain the deformed shape.

$$\{F_i\} = [k_{11} \quad k_{21} \quad k_{31} \quad k_{41} \quad k_{51} \quad k_{61}]^T$$

Hence, an individual stiffness coefficient k_{ij} can be interpreted as the nodal force in the direction of DOF i that results from a unit displacement in the direction of DOF j, while all other DOF are set equal to zero. The physical system is illustrated in Fig. 19.4.

Equivalent Nodal Load Vector: The Constant Strain Triangle

Assume that body forces are applied to the CST element (surface tractions will be considered subsequently). The virtual work δW_B of the body forces on the element during an arbitrary virtual displacement $\{\delta u\}$ is given by Eq. (19.7). Substitution

TABLE 19.1
CST Element Stiffness Matrix, Plane Stress Case (Partitioned into 2 × 2 Nodal Submatrices)

column index $j \rightarrow$ (1 2 3 4 5 6); row index $i \downarrow$

$$C \begin{bmatrix}
y_{23}^2 + \frac{1-\nu}{2}x_{32}^2 & \frac{1+\nu}{2}x_{32}y_{23} & y_{31}y_{23} + \frac{1+\nu}{2}x_{13}x_{32} & \nu x_{13}y_{23} + \frac{1-\nu}{2}x_{32}y_{31} & y_{12}y_{23} + \frac{1-\nu}{2}x_{21}x_{32} & \nu x_{21}y_{23} + \frac{1-\nu}{2}x_{32}y_{12} & 1 \\
\frac{1+\nu}{2}x_{32}y_{23} & x_{32}^2 + \frac{1-\nu}{2}y_{23}^2 & \nu x_{32}y_{31} + \frac{1-\nu}{2}x_{13}y_{23} & x_{13}x_{32} + \frac{1-\nu}{2}y_{23}y_{31} & \nu x_{32}y_{12} + \frac{1-\nu}{2}x_{21}y_{23} & x_{21}x_{32} + \frac{1-\nu}{2}y_{12}y_{23} & 2 \\
y_{31}y_{23} + \frac{1+\nu}{2}x_{13}x_{32} & \nu x_{32}y_{31} + \frac{1-\nu}{2}x_{13}y_{23} & y_{31}^2 + \frac{1-\nu}{2}x_{13}^2 & \frac{1+\nu}{2}x_{13}y_{31} & y_{12}y_{31} + \frac{1-\nu}{2}x_{13}x_{21} & \nu x_{21}y_{31} + \frac{1-\nu}{2}x_{13}y_{12} & 3 \\
\nu x_{13}y_{23} + \frac{1-\nu}{2}x_{32}y_{31} & x_{13}x_{32} + \frac{1-\nu}{2}y_{23}y_{31} & \frac{1+\nu}{2}x_{13}y_{31} & x_{13}^2 + \frac{1-\nu}{2}y_{31}^2 & \nu x_{13}y_{12} + \frac{1-\nu}{2}x_{21}y_{31} & x_{13}x_{21} + \frac{1-\nu}{2}y_{12}y_{31} & 4 \\
y_{12}y_{23} + \frac{1-\nu}{2}x_{21}x_{32} & \nu x_{32}y_{12} + \frac{1-\nu}{2}x_{21}y_{23} & y_{12}y_{31} + \frac{1-\nu}{2}x_{13}x_{21} & \nu x_{13}y_{12} + \frac{1-\nu}{2}x_{21}y_{31} & y_{12}^2 + \frac{1-\nu}{2}x_{21}^2 & \frac{1+\nu}{2}x_{21}y_{12} & 5 \\
\nu x_{21}y_{23} + \frac{1-\nu}{2}x_{32}y_{12} & x_{21}x_{32} + \frac{1-\nu}{2}y_{12}y_{23} & \nu x_{21}y_{31} + \frac{1-\nu}{2}x_{13}y_{12} & x_{13}x_{21} + \frac{1-\nu}{2}y_{12}y_{31} & \frac{1+\nu}{2}x_{21}y_{12} & x_{21}^2 + \frac{1-\nu}{2}y_{12}^2 & 6
\end{bmatrix}$$

$$C = \frac{Et}{4A(1-\nu^2)}, \qquad x_{ij} = x_i - x_j, \qquad y_{ij} = y_i - y_j$$

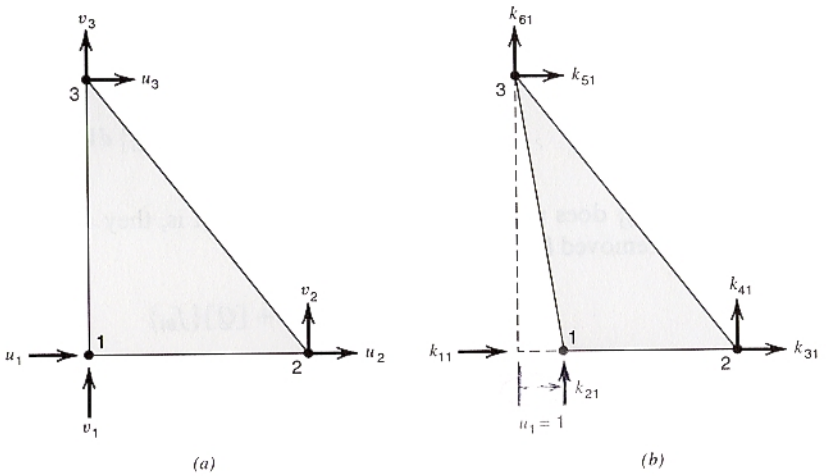

Figure 19.4 Physical interpretation of k_{ij}. (*a*) Undeformed element. (*b*) Deformed element, forces k_{i1} required to maintain $u_1 = 1$.

of Eq. (19.23) into Eq. (19.7) gives

$$\delta W_B = \{\delta u_i\}^T \int_V [N]^T \{F_B\}\, dV \tag{19.33}$$

The total external virtual work δW is the sum of the virtual work of the body forces and the virtual work of the concentrated forces so that Eq. (19.29) becomes

$$\{\delta u_i\}^T \left(\{F_i\} + \int_V [N]^T \{F_B\}\, dV - \left[\int_V [B]^T [D][B]\, dV \right] \{u_i\} \right) = 0 \tag{19.34}$$

Comparison of Eq. (19.34) with Eq. (19.29) shows that, with the addition of body forces, the load vector for the element is now

$$\{P_i\} = \{F_i\} + \int_V [N]^T \{F_B\}\, dV \tag{19.35}$$

The vector $\{P_i\}$ is the equivalent nodal load vector for the element. That is, the work of the loads $\{P_i\}$ under the virtual displacement $\{\delta u_i\}$ of the nodes is equivalent to the work of the actual concentrated loads and body forces under the virtual displacement $\{\delta u\}$.

In Eq. (19.35), the body force $\{F_B\}$ is expressed as a continuous function of the spatial coordinates. However, when constructing a finite element model, it is customary for the analyst to define element loads in terms of the intensity of the load at the nodes, rather than in functional form. The nodal force intensity is simply the magnitude of the body force at the node. Thus, for convenience, assume that the body force distribution may be expressed in terms of the force intensities at the nodes according to the relation

$$\{F_B\} = [N]\{f_{Bi}\}$$

where $\{f_{Bi}\}$ is the vector of nodal force intensities. Substitution of this relation into Eq. (19.35) gives

$$\{P_i\} = \{F_i\} + \int_V [N]^T[N]\{f_{Bi}\}\,dV$$

Since $\{f_{Bi}\}$ does not vary over the element, that is, they are nodal quantities that can be removed from the integral,

$$\{P_i\} = \{F_i\} + [Q]\{f_{Bi}\} \tag{19.36}$$

where

$$[Q] = \int_V [N]^T[N]\,dV$$

Thus, for a CST element,

$$[Q] = \frac{At}{9}\begin{bmatrix} 1 & 0 & 1 & 0 & 1 & 0 \\ 0 & 1 & 0 & 1 & 0 & 1 \\ 1 & 0 & 1 & 0 & 1 & 0 \\ 0 & 1 & 0 & 1 & 0 & 1 \\ 1 & 0 & 1 & 0 & 1 & 0 \\ 0 & 1 & 0 & 1 & 0 & 1 \end{bmatrix}$$

Now suppose that, in addition to concentrated nodal loads and body forces, the element is subjected to surface tractions along a single edge and that the continuous load function $\{F_S\}$ is expressed in terms of the nodal force intensities $\{f_{Si}\}$ by use of the shape functions. Since only one edge is loaded, only two of the nodes have nodal intensities and only these two nodes have equivalent nodal load components. Hence, for these two nodes, the interpolation equation is

$$\{\bar{F}_S\} = [\bar{N}]\{\bar{f}_{Si}\}$$

where the overbar indicates that only these two element nodes are included in the equation.

By the same approach as for body forces, the equivalent nodal loads due to surface traction on one edge are

$$\{\bar{P}_i\} = [\bar{Q}]\{\bar{f}_{Si}\} \tag{19.37}$$

where

$$[\bar{Q}] = \int_S [\bar{N}]^T[\bar{N}]\,dS \tag{19.38}$$

and the integral is evaluated over the loaded edge, where $dS = t\,ds$, t = thickness and s is a coordinate along the loaded edge. The equivalent nodal load vector $\{\bar{P}_i\}$ in Eq. (19.37) is then added to $\{P_i\}$ from Eq. (19.36), but first it must be expanded from four to six terms to account for the fact that one node does not participate in the loading.

EXAMPLE 19.1
Equivalent Nodal Loads for Linear Surface Traction

A horizontally directed, linearly varying surface traction is applied to edge 1–3 of the CST element with nodal intensities as shown in Fig. E19.1. Determine the vector of equivalent nodal loads for the element.

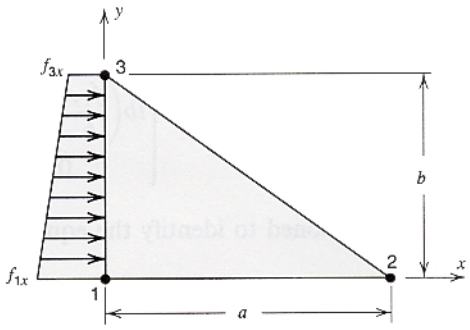

Figure E19.1

SOLUTION

The surface traction function is interpolated from the nodal intensities at nodes 1 and 3 the corresponding shape functions

$$f_x(y) = N_1 f_{1x} + N_3 f_{3x} \tag{a}$$

With the coordinates of the nodes, the shape functions are simplified to

$$N_1 = 1 - \frac{y}{b}, \qquad N_3 = \frac{y}{b} \tag{b}$$

By Eq. (19.38), with $ds = dy$,

$$[\bar{Q}] = t \int_0^b \begin{bmatrix} N_1^2 & 0 & N_1 N_3 & 0 \\ 0 & N_1^2 & 0 & N_1 N_3 \\ N_1 N_3 & 0 & N_3^2 & 0 \\ 0 & N_1 N_3 & 0 & N_3^2 \end{bmatrix} dy \tag{c}$$

By Eqs. (b) and (c),

$$[\bar{Q}] = t \begin{bmatrix} \frac{b}{3} & 0 & \frac{b}{6} & 0 \\ 0 & \frac{b}{3} & 0 & \frac{b}{6} \\ \frac{b}{6} & 0 & \frac{b}{3} & 0 \\ 0 & \frac{b}{6} & 0 & \frac{b}{3} \end{bmatrix} \tag{d}$$

and by Eq. (a), the vector of nodal intensities $\{\bar{f}_{Si}\}$ is

$$\{\bar{f}_{Si}\} = [f_{1x} \quad 0 \quad f_{3x} \quad 0]^T \tag{e}$$

With Eqs. (d) and (e), the equivalent nodal load vector $\{\bar{P}_i\}$ is obtained from Eq. (19.37) as

$$\{\bar{P}_i\} = \begin{Bmatrix} tb\left(\frac{f_{1x}}{3} + \frac{f_{3x}}{6}\right) \\ 0 \\ tb\left(\frac{f_{1x}}{6} + \frac{f_{3x}}{3}\right) \\ 0 \end{Bmatrix} \tag{f}$$

Equation (e) is partitioned to identify the equivalent nodal loads associated with nodes 1 and 3.

If the vector $\{\bar{P}_i\}$ is expanded to include positions for node 2, it becomes

$$\{P_i\} = \begin{Bmatrix} tb\left(\frac{f_{1x}}{3} + \frac{f_{3x}}{6}\right) \\ 0 \\ 0 \\ 0 \\ tb\left(\frac{f_{1x}}{6} + \frac{f_{3x}}{3}\right) \\ 0 \end{Bmatrix}$$

Assembly of the Structure Stiffness Matrix and Load Vector

To solve a plane elasticity problem by the finite element method, it is necessary to combine the individual element stiffness matrices $[K]_j$ and load vectors $\{P\}_j$ to form the *structure stiffness matrix* $[\boldsymbol{K}]$ and *structure load vector* $\{\boldsymbol{P}\}$, respectively. To demonstrate the logic associated with the assembly process, two node numbering systems for the nodes are used. Let numerals in boldface refer to the nodes of the structural system and numerals in lightface the nodes for a particular element. Likewise, lightface $[K]$, $\{u_i\}$, and $\{P_i\}$ refer to element quantities, whereas boldface $[\boldsymbol{K}]$, $\{\boldsymbol{u}_i\}$, and $\{\boldsymbol{P}_i\}$ refer to structure quantities. A specific two-dimensional discretization is shown in Fig. 19.5 to illustrate the node numbering. For this model, there are 6 structure nodes but a total of 12 separate element nodes. The assembly process involves assigning unique identifiers to each of the nodes in the model, using the structure node numbering, and then combining element stiffness matrices and load vectors according to the numbering.

For purposes of demonstration, we consider first a mathematically precise, but computationally inefficient, approach for this assembly. Then, we discuss an approach that is more appropriate for computer implementation.

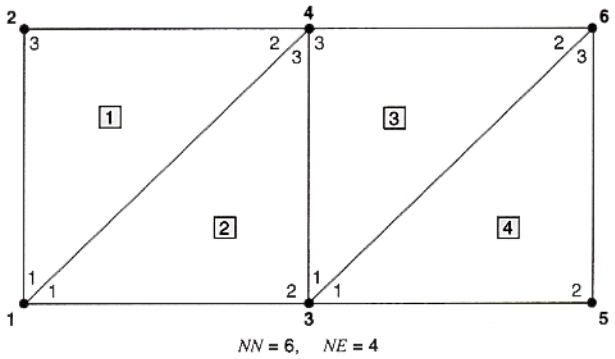

Figure 19.5 Assembly of CST elements.

For element j, define a matrix $[M]_j$ with order $(6 \times 2NN)$*, where NN is the number of nodes in the structure, to define the mapping from the element DOF vector $\{u_i\}_j$, with order (6×1), to the structure DOF vector $\{\boldsymbol{u}_i\}$, with order $(2NN \times 1)$.

$$\{u_i\}_j = [M]_j\{\boldsymbol{u}_i\} \tag{19.39}$$

By Fig. 19.5, the mapping for element 1 takes the form

$$\{u_i\}_1 = [u_1 \quad v_1 \quad u_2 \quad v_2 \quad u_3 \quad v_3]_1^T$$
$$\{\boldsymbol{u}_i\} = [u_1 \quad v_1 \quad u_2 \quad v_2 \quad u_3 \quad v_3 \quad \cdots \quad v_6]^T$$

and

$$[M]_1 = \begin{bmatrix} 1 & 0 & 0 & 0 & 0 & 0 & 0 & 0 & 0 & 0 & 0 & 0 \\ 0 & 1 & 0 & 0 & 0 & 0 & 0 & 0 & 0 & 0 & 0 & 0 \\ 0 & 0 & 0 & 0 & 0 & 0 & 1 & 0 & 0 & 0 & 0 & 0 \\ 0 & 0 & 0 & 0 & 0 & 0 & 0 & 1 & 0 & 0 & 0 & 0 \\ 0 & 0 & 1 & 0 & 0 & 0 & 0 & 0 & 0 & 0 & 0 & 0 \\ 0 & 0 & 0 & 1 & 0 & 0 & 0 & 0 & 0 & 0 & 0 & 0 \end{bmatrix}$$

By inspection or by Eq. (19.39), the DOF mapping for element 1 is

$$[u_1 \quad v_1 \quad u_2 \quad v_2 \quad u_3 \quad v_3]_1^T \leftrightarrow [u_1 \quad v_1 \quad u_4 \quad v_4 \quad u_2 \quad v_2]^T$$

The double-headed arrow indicates the reversibility of the mapping of the quantities on the left to the quantities on the right. Nodal forces and stiffness coefficients for element 1 follow the same mapping.

Next, the virtual work expressions for the entire structure are written as the sum of the virtual work for all elements

$$\sum_{j=1}^{NE} \{\delta u_i\}_j^T \{F_i\}_j + \sum_{j=1}^{NE} \{\delta u_i\}_j^T \int_S [\bar{N}]_j^T \{F_S\}_j \, dS$$
$$+ \sum_{j=1}^{NE} \{\delta u_i\}_j^T \int_V [N]_j^T \{F_B\}_j \, dV - \sum_{j=1}^{NE} \{\delta u_i\}_j^T [K]_j \{u_i\}_j = 0 \tag{19.40}$$

* The matrix $[M]_j$ in known as a *Boolean connectivity matrix* since it contains only ones and zeros.

where NE is the number of elements in the model. Substitution of Eq. (19.39) into Eq. (19.40) for each element gives

$$\{\delta \boldsymbol{u}_i\}^T \sum_{j=1}^{NE} [M]_j^T \{F_i\}_j + \{\delta \boldsymbol{u}_i\}^T \sum_{j=1}^{NE} [\bar{M}]_j^T \int_S [\bar{N}]_j^T \{F_S\}_j \, dS + \{\delta \boldsymbol{u}_i\}^T \sum_{j=1}^{NE} [M]_j^T \int_V [N]_j^T \{F_B\}_j \, dV - \{\delta \boldsymbol{u}_i\}^T \left[\sum_{j=1}^{NE} [M]_j^T [K]_j [M]_j \right] \{\boldsymbol{u}_i\} = 0 \tag{19.41}$$

Since $\{\delta \boldsymbol{u}_i\}$ is arbitrary, it is eliminated from Eq. (19.41) to obtain

$$[\boldsymbol{K}]\{\boldsymbol{u}_i\} = \{\boldsymbol{P}_i\} \tag{19.42a}$$

where

$$[\boldsymbol{K}] = \left[\sum_{j=1}^{NE} [M]_j^T [K]_j [M]_j \right] \tag{19.42b}$$

and

$$\{\boldsymbol{P}_i\} = \sum_{j=1}^{NE} [M]_j^T \{F_i\}_j + \sum_{j=1}^{NE} [\bar{M}]_j^T \int_S [\bar{N}]_j^T \{F_S\}_j \, dS + \sum_{j=1}^{NE} [M]_j^T \int_V [N]_j^T \{F_B\}_j \, dV \tag{19.42c}$$

In Eqs. (19.41) and (19.42c), matrix $[\bar{M}]_j$, of order $(4 \times 2NN)$, accounts for the mapping to the structure nodes of the two nodes in element j that participate in the surface tractions. If more than one edge on an element is loaded, then Eqs. (19.41) and (19.42c) are extended accordingly.

The forms of $[\boldsymbol{K}]$ and $\{\boldsymbol{P}_i\}$ in Eq. (19.42) are precise but they are not used in practice. The matrix products involving $[M]_j$, which involve multiplying by 0 or 1, do nothing more than move individual quantities from one position in the element stiffness matrix or load vector to another in the structure stiffness matrix or load vector. Although the above development is not practical, it does demonstrate that the structure stiffness matrix is assembled by successively adding the stiffness terms from each element into appropriate locations of the structure matrix; the same is true for the structure load vector. A more direct approach to assembly is demonstrated in Example 19.2.

EXAMPLE 19.2
Assembly of the Structure Stiffness Matrix

For the model shown in Fig. 19.5, illustrate the assembly of the stiffness matrix for element 1 into the structure stiffness matrix.

SOLUTION

Since the structure has six nodes, each of which has two DOF, the structure stiffness matrix is of order (12×12). The individual stiffness coefficients are designated k_{ij}^e, where now the superscript identifies the element number. With this notation, the stiffness matrix for element 1 is shown in Fig. E19.2. The mapping of element

$$[K]_1 = \begin{bmatrix} k_{11}^1 & k_{12}^1 & k_{13}^1 & k_{14}^1 & k_{15}^1 & k_{16}^1 \\ \bullet & & \circ & & \blacklozenge & \\ k_{21}^1 & k_{22}^1 & k_{23}^1 & k_{24}^1 & k_{25}^1 & k_{26}^1 \\ k_{31}^1 & k_{32}^1 & k_{33}^1 & k_{34}^1 & k_{35}^1 & k_{36}^1 \\ \blacktriangledown & & \blacktriangle & & \triangle & \\ k_{41}^1 & k_{42}^1 & k_{43}^1 & k_{44}^1 & k_{45}^1 & k_{46}^1 \\ k_{51}^1 & k_{52}^1 & k_{53}^1 & k_{54}^1 & k_{55}^1 & k_{56}^1 \\ \triangledown & & \square & & \blacksquare & \\ k_{61}^1 & k_{62}^1 & k_{63}^1 & k_{64}^1 & k_{65}^1 & k_{66}^1 \end{bmatrix}$$

(*a*)

$$[K] = \begin{bmatrix} k_{11}^1 & k_{12}^1 & k_{15}^1 & k_{16}^1 & & k_{13}^1 & k_{14}^1 & & \\ \bullet & & \blacklozenge & & & \circ & & & \\ k_{21}^1 & k_{22}^1 & k_{25}^1 & k_{26}^1 & & k_{23}^1 & k_{24}^1 & & \\ k_{51}^1 & k_{52}^1 & k_{55}^1 & k_{56}^1 & & k_{53}^1 & k_{54}^1 & & \\ \triangledown & & \blacksquare & & & \square & & & \\ k_{61}^1 & k_{62}^1 & k_{65}^1 & k_{66}^1 & & k_{63}^1 & k_{64}^1 & & \\ & & & & & & & & \\ k_{31}^1 & k_{32}^1 & k_{35}^1 & k_{36}^1 & & k_{33}^1 & k_{34}^1 & & \\ \blacktriangledown & & \triangle & & & \blacktriangle & & & \\ k_{41}^1 & k_{42}^1 & k_{45}^1 & k_{46}^1 & & k_{43}^1 & k_{44}^1 & & \\ & & & & & & & & \\ & & & & & & & & \\ & & & & & & & & \end{bmatrix}$$

(*b*)

Figure E19.2 Assembly of element 1 stiffness matrix (with 2×2 nodal submatrix partitions). (*a*) Stiffness matrix for element 1. (*b*) Structure stiffness matrix with element 1 assembled.

TABLE E19.2
Element to Structure Node Mapping

	Structure Node Numbers			
Element Node No.	**Element 1**	**Element 2**	**Element 3**	**Element 4**
1	**1**	**1**	**3**	**3**
2	**4**	**3**	**6**	**5**
3	**2**	**4**	**4**	**6**

node numbers to structure node numbers is determined by inspection of the model in Fig. 19.5 and is summarized in Table E19.2. The list of structure node numbers that define the nodes for each element is commonly known as the *incidence list*. The incidence list is one of the input requirements for finite element programs. Using the incidence list, one can obtain the mapping of the element 1 nodal submatrices into the structure stiffness matrix (Fig. E19.2). Markers have been added to the nodal submatrices as an aid to visualization of the placement of element stiffness coefficients into the structure stiffness matrix.

As described in the previous example, the incidence list is used to drive the assembly process. Suppose that the node numbers that comprise the incidence list (e.g., Table E19.2) are placed into a matrix $[INCID]$ that contains one column for each element. The i, j term in the matrix is defined as the structure node number that corresponds to element node number i of element j. Then, by using the incidence matrix $[INCID]$, each term from the element stiffness matrix $[K]_j$ is moved into the structure stiffness matrix $[\boldsymbol{K}]$ in a prescribed manner. The method is illustrated by a Fortran subroutine in Table 19.2. The subroutine moves one nodal submatrix at a time. Note that this code is for illustrative purposes only. Because of the symmetry and sparsity of the structure stiffness matrix, it is usually stored in some form other than a square matrix.

Application of Constraints

The model shown in Fig. 19.5 is not fastened to supports. Hence, it represents an unstable structure, a structure that is not capable of resisting external loads. The assembled stiffness matrix for an unstable structure is singular; it has a rank deficiency of 3 due to the three rigid-body modes that the model possesses. Physically, the structure must be supported to prevent rigid-body motion. In a like fashion, if the structure stiffness matrix is modified to reflect the support conditions (commonly known as constraints), it becomes nonsingular. Several methods may be used to apply constraints to the structure stiffness matrix. Only one, the so-called *equation modification method*, will be discussed here.

To demonstrate the equation modification method, consider a model that contains only a single element (Fig. 19.6*a*). The first step is to switch appropriate rows and columns of the stiffness such that those DOF that are constrained are grouped together. The rearranged stiffness matrix, displacement vector, and load vector for the one-element model are shown in Fig. 19.6*b*. For simplicity, the rearranged equations are represented in the symbolic form

$$\left[\begin{array}{c|c} \boldsymbol{K}_{cc} & \boldsymbol{K}_{cu} \\ \hline \boldsymbol{K}_{uc} & \boldsymbol{K}_{uu} \end{array}\right] \left\{\begin{array}{c} \boldsymbol{u}_c \\ \hline \boldsymbol{u}_u \end{array}\right\} = \left\{\begin{array}{c} \boldsymbol{P}_c \\ \hline \boldsymbol{P}_u \end{array}\right\} \tag{19.43}$$

where the subscript c represents the constrained DOF and the subscript u the unconstrained DOF.* The relationship between the submatrices and subvectors in

* The rearrangement of the equations and subsequent partitioning are done for convenience in representing the method. Computer implementation of this approach does not require that the equations be rearranged, nor would such rearrangement be computationally efficient.

TABLE 19.2
FORTRAN Subroutine for Stiffness Assembly

```
      SUBROUTINE ASSMBL(KS,KE,NNE,NDOF,INCID,IE,NRS,NRE,NE)
      DIMENSION KS(NRS, NRS), KE(NRE, NR), INCID(NNE, NE)
      REAL KS, KE
C
C         ASSEMBLE THE STIFFNESS FOR ELEMENT 'IE' INTO THE
C         STRUCTURE STIFFNESS.
C
C     CONTROL VARIABLES:
C
C  KS, KE    = STRUCTURE & ELEMENT STIFFNESS MATRICES.
C  NNE       = NUMBER OF NODES IN AN ELEMENT.
C  NDOF      = NUMBER OF DOF AT EACH NODE.
C  INCID     = INCIDENCE MATRIX.
C  IE        = CURRENT ELEMENT NUMBER.
C  NRS, NRE  = NUMBER OF ROWS IN STRUCTURE & ELEMENT STIFFNESS
C  NE        = NUMBER OF ELEMENTS IN THE MODEL.
C
C     LOCAL VARIABLES:
C
C  INE  = CURRENT ELEMENT SUBMATRIX ROW NUMBER.
C  JNE  = CURRENT ELEMENT SUBMATRIX COLUMN NUMBER.
C  INS  = CURRENT STRUCTURE SUBMATRIX ROW NUMBER.
C  JNS  = CURRENT STRUCTURE SUBMATRIX COLUMN NUMBER.
C  IDOF = CURRENT DOF NUMBER IN SUBMATRIX ROW.
C  JDOF = CURRENT DOF NUMBER IN SUBMATRIX COLUMN.
C  IKE  = ROW ENTRY IN THE ELEMENT STIFFNESS.
C  JKE  = COLUMN ENTRY IN THE ELEMENT STIFFNESS.
C  IKS  = ROW ENTRY IN THE STRUCTURE STIFFNESS.
C  JKS  = COLUMN ENTRY IN THE STRUCTURE STIFFNESS.
C
      DO 10 INE = 1, NNE
         INS = INCID( INE, IE )
      DO 10 JNE = 1, NNE
         JNS = INCID( JNE, IE )
C
C         ASSEMBLE THE ELEMENT SUBMATRIX (INE,JNE) INTO
C         THE STRUCTURE SUBMATRIX (INS, JNS)
C
      DO 10 IDOF = 1, NDOF
         IKE = ( INE - 1 ) * NDOF + IDOF
         IKS = ( INS - 1 ) * NDOF + IDOF
      DO 10 JDOF = 1, NDOF
         JKE = ( JNE - 1 ) * NDOF + JDOF
         JKS = ( JNS - 1 ) * NDOF + JDOF
C
         KS( IKS, JKS ) = KS( IKS, JKS ) + KE( IKE, JKE )
C
   10 CONTINUE
      RETURN
      END
```

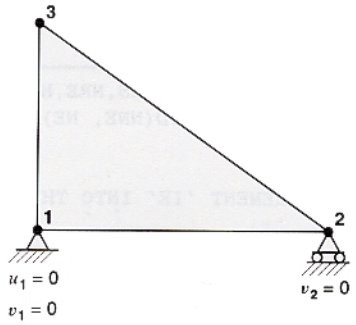

(a)

$$\left[\begin{array}{ccc:ccc} k_{11} & k_{12} & k_{14} & k_{13} & k_{15} & k_{16} \\ k_{21} & k_{22} & k_{24} & k_{23} & k_{25} & k_{26} \\ k_{41} & k_{42} & k_{44} & k_{43} & k_{45} & k_{46} \\ \hdashline k_{31} & k_{32} & k_{34} & k_{33} & k_{35} & k_{36} \\ k_{51} & k_{52} & k_{54} & k_{53} & k_{55} & k_{56} \\ k_{61} & k_{62} & k_{64} & k_{63} & k_{65} & k_{66} \end{array}\right] \left\{\begin{array}{c} u_1 \\ v_1 \\ v_2 \\ \hdashline u_2 \\ u_3 \\ v_3 \end{array}\right\} = \left\{\begin{array}{c} P_{1x} \\ P_{1y} \\ P_{2y} \\ \hdashline P_{2x} \\ P_{3x} \\ P_{3y} \end{array}\right\}$$

(b)

Figure 19.6 Application of constraints by the equation modification method. (*a*) One-element model with constraints. (*b*) Rearranged structure equations.

Eq. (19.43) and those in Fig. 19.6*b* is determined by their respective positions in the equations.

The unknown quantities are the displacements $\{\boldsymbol{u}_u\}$ of the unconstrained DOF and the forces $\{\boldsymbol{P}_c\}$ at the constrained DOF. Rewrite Eq. (19.43) as two separate submatrix/subvector equations.

$$[\boldsymbol{K}_{cc}]\{\boldsymbol{u}_c\} + [\boldsymbol{K}_{cu}]\{\boldsymbol{u}_u\} = \{\boldsymbol{P}_c\} \tag{19.44a}$$

$$[\boldsymbol{K}_{uc}]\{\boldsymbol{u}_c\} + [\boldsymbol{K}_{uu}]\{\boldsymbol{u}_u\} = \{\boldsymbol{P}_u\} \tag{19.44b}$$

Since $\{\boldsymbol{u}_c\}$ is known, it is moved to the load side of Eq. (19.44b) to obtain

$$[\boldsymbol{K}_{uu}]\{\boldsymbol{u}_u\} = \{\boldsymbol{P}_u\} - [\boldsymbol{K}_{uc}]\{\boldsymbol{u}_c\} \tag{19.45}$$

Equation (19.45) is the constrained system of equations. If the imposed constraints $\{\boldsymbol{u}_c\}$ are nonzero, they serve to modify the load vector. If the constraints are all zero, such as in Fig. 19.6*a*, then the second term on the right side of Eq. (19.45) vanishes. In either case, the system of equations is reduced in order by the number of constrained DOF. If appropriate constraints are applied to render the structure stable, then $[\boldsymbol{K}_{uu}]$ will be nonsingular.

Solution of the System of Equations

After assembly of the stiffness matrix and load vector and application of constraints, the system of linear algebraic equations may be solved. It is common to represent the solution of Eq. (19.45) in the symbolic form

$$\{\boldsymbol{u}_u\} = [\boldsymbol{K}_{uu}]^{-1}(\{\boldsymbol{P}_u\} - [\boldsymbol{K}_{uc}]\{\boldsymbol{u}_c\})$$

However, inversion of the stiffness matrix $[\boldsymbol{K}_{uu}]$ is computationally expensive and can lead to significant numerical error. A more efficient approach, known as *Choleski decomposition*, involves triangular factorization of the stiffness matrix.

$$[\boldsymbol{K}_{uu}] = [\boldsymbol{U}]^T[\boldsymbol{U}]$$

where $[\boldsymbol{U}]$ is an upper triangular matrix; that is, each term in the lower triangle of $[\boldsymbol{U}]$ is zero ($u_{ij} = 0$, $i > j$). Factorization of $[\boldsymbol{K}_{uu}]$ into this form permits direct

solution for displacements via two *load-pass* operations. The first of these, known as the *forward load-pass*, yields an intermediate solution vector $\{y\}$.

$$[U]^T\{y\} = \{P_u\} - [K_{uc}]\{u_c\}$$

The second operation, known as the *backward load-pass*, produces the final displacement vector $\{u_u\}$.

$$[U]\{u_u\} = \{y\}$$

Upon solution for $\{u_u\}$, the reactions that result from deformation of the structure can be found from Eq. (19.44a). The total reactions are obtained by subtracting any nodal loads that are applied to the constrained DOF. Such loads frequently exist when element loads, in the form of body forces or surface tractions, are resolved into equivalent nodal loads.

Details of the equation solving methods and discussions of their advantages and disadvantages can be found in books that specialize in the finite element method (see the references at the end of this chapter).

19.3 THE BILINEAR RECTANGLE

The constant strain triangle is the simplest element that can be used for plane elasticity problems. As such, it is an attractive choice for demonstration of the basic formulation of the finite element method. However, because of its simplicity, the CST element exhibits relatively poor performance in a coarse mesh (a few large elements). In order to obtain satisfactory results with the CST element, a very highly refined mesh (many small elements) is generally needed for all but the most trivial problems. Alternatively, one may use a different element that is based on different displacement interpolation functions and that yields better results. The number of alternatives to the CST element is quite large and no attempt is made to discuss all of them here. Instead, we examine two alternatives: the bilinear rectangle and the linear isoparametric quadrilateral. The development of the bilinear rectangle follows. The linear isoparametric quadrilateral is presented in Sec. 19.4.

Consider a rectangular element of width $2a$, height $2b$, and with corner nodes numbered in a counterclockwise order. The (x, y) coordinate axes for the element are parallel to the 1–2 and 1–4 edges of the element, respectively, and the origin of the coordinate system is at the centroid of the element (see Fig. 19.7). As with the CST element, the displacement components (u, v) at any point P are expressed in terms of the nodal displacements. Since there are four nodes in the element, each with two nodal DOF, the displacement functions for $u(x, y)$ and $v(x, y)$ each have four coefficients. Hence, we choose the bilinear functions*

$$u(x, y) = a_1 + a_2x + a_3y + a_4xy$$
$$v(x, y) = a_5 + a_6x + a_7y + a_8xy$$

* These functions are said to be bilinear functions of (x, y) because the dependency on x and y comes from the product of two linear expressions, one in x and one in y. The corresponding rectangular element is said to be bilinear. With the given functions (u, v), the straight edges of the bilinear rectangle remain straight under deformation (like the CST element). However, the strain components in the bilinear rectangle element are not constant.

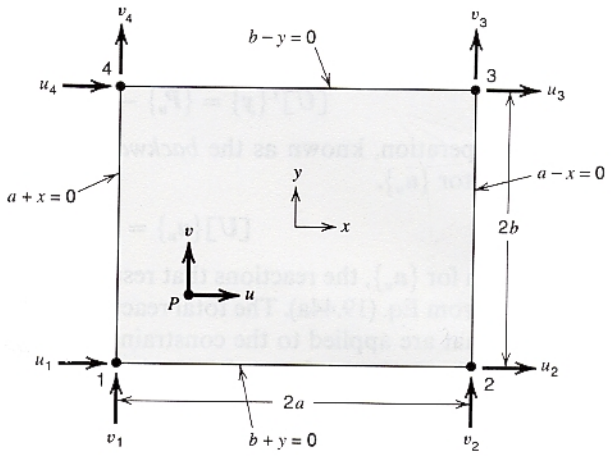

Figure 19.7 Bilinear rectangle element.

Like the CST element, the bilinear rectangle can properly represent rigid-body translation, rigid-body rotation, and constant strain. The bilinear displacement components (a_4xy and a_8xy) result in strain components such that ϵ_{xx} is linear in y, ϵ_{yy} is linear in x, and γ_{xy} is linear in both x and y. This higher-order response, compared to the CST element, results in more efficient and accurate numerical solutions.

Development of the stiffness matrix and load vector proceeds in a manner similar to that for the CST element. Only the stiffness matrix is developed here; development of the load vector is left as an exercise for the reader. The shape functions are expressed as products of one-dimensional Lagrange interpolation functions (Kellison, 1975)

$$N_1(x,y) = \frac{(a-x)(b-y)}{4ab}$$

$$N_2(x,y) = \frac{(a+x)(b-y)}{4ab}$$

$$N_3(x,y) = \frac{(a+x)(b+y)}{4ab}$$

$$N_4(x,y) = \frac{(a-x)(b+y)}{4ab} \tag{19.46}$$

Since the shape function for node i has zero value along any element edge that does not include node i, the shape function can be derived directly as the product of the equations of the lines that define these edges; see Fig. 19.7. The shape functions for the bilinear rectangle are illustrated in Fig. 19.8 where they form straight lines along the element edges. However, over the interior of the element, the functions form curved surfaces, with linearly varying slopes in the x and y directions.

The strain-displacement relations are written in the form of Eq. (19.25), with the nodal displacement vector

$$\{u_i\} = [u_1 \quad v_1 \quad u_2 \quad v_2 \quad u_3 \quad v_3 \quad u_4 \quad v_4]^T$$

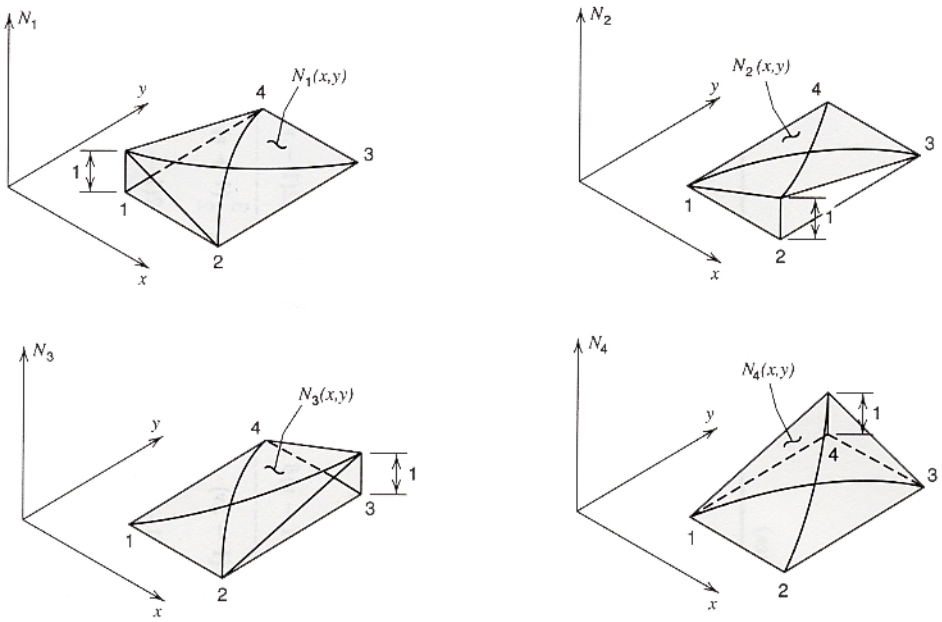

Figure 19.8 Graphical representation of shape functions for the bilinear rectangle element.

and $[B]$ matrix

$$[B] = [B_1 \quad B_2 \quad B_3 \quad B_4] \tag{19.47}$$

where for node i

$$[B_i] = \begin{bmatrix} \dfrac{\partial N_i}{\partial x} & 0 \\ 0 & \dfrac{\partial N_i}{\partial y} \\ \dfrac{\partial N_i}{\partial y} & \dfrac{\partial N_i}{\partial x} \end{bmatrix} \tag{19.48}$$

The element stiffness matrix is found from Eq. (19.31). That equation is repeated here with the order of each matrix shown as a subscript.

$$[K]_{8\times 8} = \int_V [B]^T_{8\times 3}[D]_{3\times 3}[B]_{3\times 8}\, dV$$

The stiffness matrix can be written in terms of (2 × 2) nodal submatrices as

$$[K_{ij}]_{2\times 2} = \int_V [B_i]^T_{2\times 3}[D]_{3\times 3}[B_j]_{3\times 2}\, dV$$

where i and j are element node numbers. The explicit form of the bilinear rectangle element stiffness matrix for a plane stress condition is given in Table 19.3.

TABLE 19.3
Bilinear Rectangle Stiffness Matrix, Plane Stress Case (Partitioned into 2 × 2 Nodal Submatrices)

column index $j\rightarrow$ row index $i\downarrow$

$$C\begin{bmatrix}
4\beta+\frac{2(1-\nu)}{\beta} & \frac{3}{2}(1+\nu) & -4\beta+\frac{(1-\nu)}{\beta} & -\frac{3}{2}(1-3\nu) & -2\beta-\frac{(1-\nu)}{\beta} & -\frac{3}{2}(1+\nu) & 2\beta-\frac{2(1-\nu)}{\beta} & \frac{3}{2}(1-3\nu) & 1\\
\frac{3}{2}(1+\nu) & \frac{4}{\beta}+2(1-\nu)\beta & \frac{3}{2}(1-3\nu) & \frac{2}{\beta}-2(1-\nu)\beta & -\frac{3}{2}(1+\nu) & -\frac{2}{\beta}-(1-\nu)\beta & -\frac{3}{2}(1-3\nu) & -\frac{4}{\beta}+(1-\nu)\beta & 2\\
-4\beta+\frac{(1-\nu)}{\beta} & \frac{3}{2}(1-3\nu) & 4\beta+\frac{2(1-\nu)}{\beta} & -\frac{3}{2}(1+\nu) & 2\beta-\frac{2(1-\nu)}{\beta} & -\frac{3}{2}(1-3\nu) & -2\beta-\frac{(1-\nu)}{\beta} & \frac{3}{2}(1+\nu) & 3\\
-\frac{3}{2}(1-3\nu) & \frac{2}{\beta}-2(1-\nu)\beta & -\frac{3}{2}(1+\nu) & \frac{4}{\beta}+2(1-\nu)\beta & \frac{3}{2}(1-3\nu) & -\frac{4}{\beta}+(1-\nu)\beta & \frac{3}{2}(1+\nu) & -\frac{2}{\beta}-(1-\nu)\beta & 4\\
-2\beta-\frac{(1-\nu)}{\beta} & -\frac{3}{2}(1+\nu) & 2\beta-\frac{2(1-\nu)}{\beta} & \frac{3}{2}(1-3\nu) & 4\beta+\frac{2(1-\nu)}{\beta} & \frac{3}{2}(1+\nu) & -4\beta+\frac{(1-\nu)}{\beta} & -\frac{3}{2}(1-3\nu) & 5\\
-\frac{3}{2}(1+\nu) & -\frac{2}{\beta}-(1-\nu)\beta & -\frac{3}{2}(1-3\nu) & -\frac{4}{\beta}+(1-\nu)\beta & \frac{3}{2}(1+\nu) & \frac{4}{\beta}+2(1-\nu)\beta & \frac{3}{2}(1-3\nu) & \frac{2}{\beta}-2(1-\nu)\beta & 6\\
2\beta-\frac{2(1-\nu)}{\beta} & -\frac{3}{2}(1-3\nu) & -2\beta-\frac{(1-\nu)}{\beta} & \frac{3}{2}(1+\nu) & -4\beta+\frac{(1-\nu)}{\beta} & \frac{3}{2}(1-3\nu) & 4\beta+\frac{2(1-\nu)}{\beta} & -\frac{3}{2}(1+\nu) & 7\\
\frac{3}{2}(1-3\nu) & -\frac{4}{\beta}+(1-\nu)\beta & \frac{3}{2}(1+\nu) & -\frac{2}{\beta}-(1-\nu)\beta & -\frac{3}{2}(1-3\nu) & \frac{2}{\beta}-2(1-\nu)\beta & -\frac{3}{2}(1+\nu) & \frac{4}{\beta}+2(1-\nu)\beta & 8
\end{bmatrix}$$

$$C=\frac{Et}{12(1-\nu^2)},\qquad \beta=\frac{b}{a}$$

By itself, the bilinear rectangle element is limited to rectangular domains. This is potentially a rather severe restriction. However, nonrectangular domains can be modeled with a combination of bilinear rectangle elements and CST elements. Since both elements represent linear displacement variation along their edges, they are compatible; that is, displacements will be continuous across element boundaries.

EXAMPLE 19.3
Performance of the Bilinear Rectangle and CST Elements

Compare the ability of the bilinear rectangle and CST elements to model in-plane bending of a thin, square plate.

SOLUTION

A square plate of width a and thickness t is considered. For simplicity, Poisson's ratio is taken as zero, $\nu = 0$. To impose a state of pure bending, displacements $u = \pm\delta$ are imposed on the corners of the plate as shown in Fig. E19.3*a*. From the

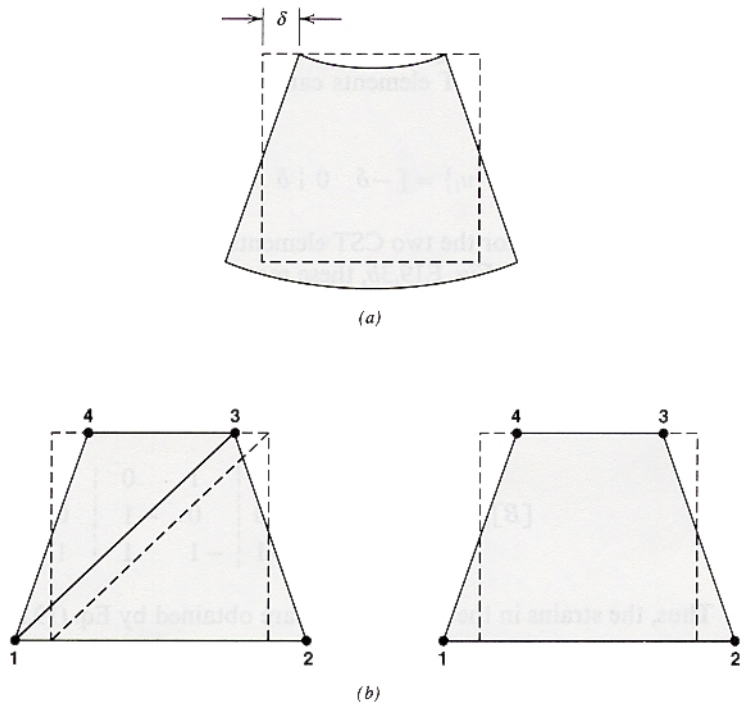

Figure E19.3 (*a*) Deformed shape (elasticity solution). (*b*) Deformed shape (finite element models).

theory of elasticity, the displacements are

$$u = -\frac{4xy\,\delta}{a^2} \tag{a}$$

$$v = \left(\frac{4x^2}{a} - 1\right)\frac{\delta}{2} \tag{b}$$

Differentiation of Eqs. (a) and (b) gives the strain components

$$\epsilon_{xx} = -\frac{4y\,\delta}{a^2}, \qquad \epsilon_{yy} = 0, \qquad \gamma_{xy} = 0 \tag{c}$$

The strain energy in the plate is

$$\begin{aligned} U &= \int_V U_0\,dV \\ &= \int_V \frac{E\epsilon_{xx}^2}{2}\,dV \\ &= \frac{2}{3}Et\,\delta^2 \end{aligned} \tag{d}$$

Two finite element models of the square plate are considered. The first uses two CST elements and the second, a single bilinear rectangle. As for the elasticity solution, nodal displacements of $u_i = \pm\delta$ are imposed. The models and their deformed shapes are shown in Fig. E19.3*b*. The model of two CST elements is considered first. Strains in the CST elements can be determined first since the displacement vector is known.

$$\{u_i\} = [-\delta \quad 0 \mid \delta \quad 0 \mid -\delta \quad 0 \mid \delta \quad 0]^T \tag{e}$$

The $[B]$ matrices for the two CST elements are defined by Eq. (19.26). For the element geometries in Fig. E19.3*b*, these matrices are

$$[B]_{CST-1} = \frac{1}{a}\left[\begin{array}{cc|cc|cc} 0 & 0 & 1 & 0 & -1 & 0 \\ 0 & -1 & 0 & 0 & 0 & 1 \\ -1 & 0 & 0 & 1 & 1 & -1 \end{array}\right] \tag{f}$$

$$[B]_{CST-2} = \frac{1}{a}\left[\begin{array}{cc|cc|cc} -1 & 0 & 1 & 0 & 0 & 0 \\ 0 & 0 & 0 & -1 & 0 & 1 \\ 0 & -1 & -1 & 1 & 1 & 0 \end{array}\right] \tag{g}$$

Thus, the strains in the two elements are obtained by Eq. (19.25) as

$$\{\epsilon\}_{CST-1} = \left[-\frac{2\delta}{a} \quad 0 \quad \frac{2\delta}{a}\right]^T \tag{h}$$

$$\{\epsilon\}_{CST-2} = \left[\frac{2\delta}{a} \quad 0 \quad -\frac{2\delta}{a}\right]^T \tag{i}$$

The structure stiffness for an assembly of two CST elements is

$$[K]_{CST} = Et \left[\begin{array}{cc|cc|cc|cc} 0.75 & 0.0 & -0.5 & 0.0 & 0.0 & -0.25 & -0.25 & 0.25 \\ 0.0 & 0.75 & 0.25 & -0.25 & -0.25 & 0.0 & 0.0 & -0.5 \\ \hline -0.5 & 0.25 & 0.75 & -0.25 & -0.25 & 0.0 & 0.0 & 0.0 \\ 0.0 & -0.25 & -0.25 & 0.75 & 0.25 & -0.5 & 0.0 & 0.0 \\ \hline 0.0 & -0.25 & -0.25 & 0.25 & 0.75 & 0.0 & -0.5 & 0.0 \\ -0.25 & 0.0 & 0.0 & -0.5 & 0.0 & 0.75 & 0.25 & -0.25 \\ \hline -0.25 & 0.0 & 0.0 & 0.0 & -0.5 & 0.25 & 0.75 & -0.25 \\ 0.25 & -0.5 & 0.0 & 0.0 & 0.0 & -0.25 & -0.25 & 0.75 \end{array}\right] \tag{j}$$

from which the product $[K]_{CST}\{u_i\}$ gives the nodal forces $\{P_i\}_{CST}$ as

$$\{P_i\}_{CST} = Et\,\delta[-1.5 \quad 0.5 \mid 1.5 \quad -0.5 \mid -1.5 \quad 0.5 \mid 1.5 \quad -0.5]^T \tag{k}$$

The strain energy in the structure is

$$U_{CST} = \tfrac{1}{2}\{u_i\}^T\{P_i\}_{CST} = 3Et\,\delta^2 \tag{l}$$

Next, consider the model with only a single bilinear rectangle shown in Fig. E19.3*b*. The $[B]$ matrix for the element is given by Eqs. (19.47) and (19.48) as

$$[B]_{BR} = \frac{1}{a^2}\left[\begin{array}{cc|cc|cc|cc} -\frac{a}{2}+y & 0 & \frac{a}{2}-y & 0 & \frac{a}{2}+y & 0 & -\frac{a}{2}-y & 0 \\ 0 & -\frac{a}{2}+x & 0 & -\frac{a}{2}-x & 0 & \frac{a}{2}+x & 0 & \frac{a}{2}-x \\ -\frac{a}{2}+x & -\frac{a}{2}+y & -\frac{a}{2}-x & \frac{a}{2}-y & \frac{a}{2}+x & \frac{a}{2}+y & \frac{a}{2}-x & -\frac{a}{2}-y \end{array}\right] \tag{m}$$

The strains are obtained by Eq. (19.25) as

$$\{\epsilon\}_{BR} = \left[-\frac{4y\,\delta}{a^2} \quad 0 \quad -\frac{4x\,\delta}{a^2}\right]^T \tag{n}$$

The stiffness matrix for the bilinear rectangle is obtained from Table (19.3), which, for this problem, becomes

$$[K]_{BR} = Et\left[\begin{array}{cc|cc|cc|cc} 0.5 & 0.125 & -0.25 & -0.125 & -0.25 & -0.125 & 0.0 & 0.125 \\ 0.125 & 0.5 & 0.125 & 0.0 & -0.125 & -0.25 & -0.125 & -0.25 \\ \hline -0.25 & 0.125 & 0.5 & -0.125 & 0.0 & -0.125 & -0.25 & 0.125 \\ -0.125 & 0.0 & -0.125 & 0.5 & 0.125 & -0.25 & 0.125 & -0.25 \\ \hline -0.25 & -0.125 & 0.0 & 0.125 & 0.5 & 0.125 & -0.25 & -0.125 \\ -0.125 & -0.25 & -0.125 & -0.25 & 0.125 & 0.5 & 0.125 & 0.0 \\ \hline 0.0 & -0.125 & -0.25 & 0.125 & -0.25 & 0.125 & 0.5 & -0.125 \\ 0.125 & -0.25 & 0.125 & -0.25 & -0.125 & 0.0 & -0.125 & 0.5 \end{array}\right] \tag{o}$$

from which the product $[K]_{BR}\{u_i\}$ gives the nodal forces $\{P_i\}_{BR}$ as

$$\{P_i\}_{BR} = Et\,\delta[-0.5 \quad 0 \;|\; 0.5 \quad 0 \;|\; -0.5 \quad 0 \;|\; 0.5 \quad 0]^T \tag{p}$$

The strain energy in the element is

$$U_{BR} = \tfrac{1}{2}\{u_i\}^T\{P_i\}_{BR} = Et\,\delta^2 \tag{q}$$

This example clearly demonstrates that the bilinear rectangle is superior to the CST element. The bilinear rectangle correctly predicts the normal strains ϵ_{xx} and ϵ_{yy}. In addition, the bilinear rectangle model stores less strain energy than the CST model. If we use the elasticity solution as the *exact* solution, $U_{BR} = 1.5U_{\text{exact}}$, whereas $U_{CST} = 4.5U_{\text{exact}}$. Notice though that both the CST and bilinear rectangle possess nonzero shear stress where none should exist. This defect, known as *parasitic* shear, contributes to excess strain energy in the elements. Although little can be done to improve the performance of the CST element, a more general formulation of the bilinear rectangle, known as the linear isoparametric quadrilateral (Sec. 19.4), can be used to control parasitic shear.

19.4 THE LINEAR ISOPARAMETRIC QUADRILATERAL

Suppose that an analyst wishes to model an irregular domain but wants to avoid the use of CST elements because of their relatively poor performance. Since the domain is irregular, the bilinear rectangle element would be inappropriate. Instead, arbitrarily shaped quadrilateral (four-sided) elements are selected to better fit boundaries. A quadrilateral element may be formulated directly, as was done above for the CST and bilinear rectangle elements. However, the necessary integrations are quite complex. This is due, in part, to the difficulty in defining the limits of integration. Use of isoparametric elements eliminates this difficulty. Isoparametric elements are formulated in *natural* coordinates as square elements and then *mapped* to physical coordinates via coordinate interpolation functions, similar to displacement interpolation functions. Depending on the type of isoparametric element used, the configuration of the element in physical coordinates can be nonrectangular and can have curved sides. If the shape functions used for coordinate interpolation are identical to those used for displacement interpolation, then the element is said to be *isoparametric*. If coordinate interpolation is of higher order than displacement interpolation (i.e., more nodes are used to represent the variation in geometry than the variation in displacements), then the element is called *superparametric*. If coordinate interpolation is of lower order than displacement interpolation (fewer nodes are used to represent the variation in geometry than the variation in displacements), then the element is called *subparametric* (Zienkiewicz and Taylor, 1989, p. 160). Because of their versatility and accuracy, isoparametric elements have become the mainstay of modern finite element programs.

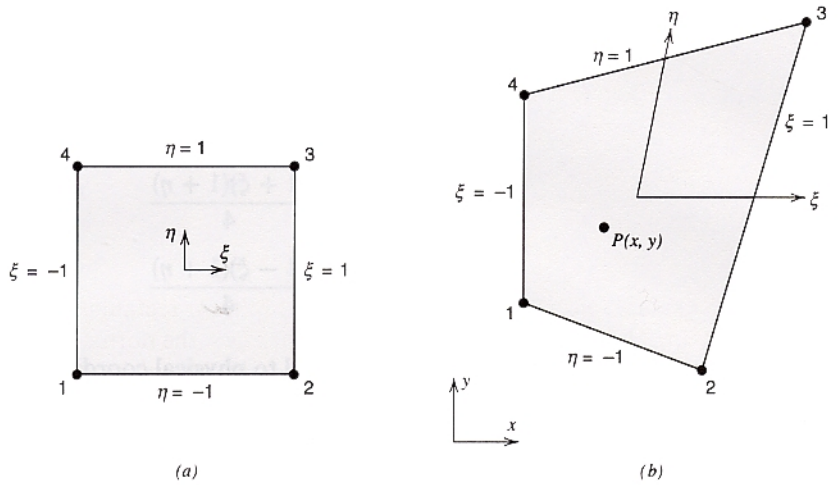

Figure 19.9 Isoparametric coordinate mapping. (*a*) Element in natural coordinates. (*b*) Element in physical coordinates.

Isoparametric Mapping

Consider the mapping of the four-node quadrilateral element from a *natural* (ξ, η) coordinate system (Fig. 19.9*a*) to a physical (x, y) coordinate system (Fig. 19.9*b*). In natural coordinates, the element is a (2×2) square and the origin of the coordinate system is at its center. In physical coordinates, the element is distorted from a rectangular shape. With shape functions in terms of the (ξ, η) coordinate system, the coordinates of any point P can be expressed in terms of the (x, y) coordinates of the nodes.

$$x(\xi, \eta) = \sum_{i=1}^{4} N_i(\xi, \eta) x_i, \qquad y(\xi, \eta) = \sum_{i=1}^{4} N_i(\xi, \eta) y_i \tag{19.49a}$$

In matrix form, Eq. (19.49a) is

$$\begin{Bmatrix} x(\xi, \eta) \\ y(\xi, \eta) \end{Bmatrix} = [N]\{x_i\} \tag{19.49b}$$

where $\{x_i\}$ is the vector of nodal coordinates

$$\{x_i\} = [x_1 \quad y_1 \quad x_2 \quad y_2 \quad x_3 \quad y_3 \quad x_4 \quad y_4]^T$$

and $[N]$ is the shape function matrix

$$[N] = \left[\begin{array}{cc|cc|cc|cc} N_1 & 0 & N_2 & 0 & N_3 & 0 & N_4 & 0 \\ 0 & N_1 & 0 & N_2 & 0 & N_3 & 0 & N_4 \end{array}\right] \tag{19.50}$$

The shape functions are the Lagrange interpolation functions [refer to Eq. (19.46)] in dimensionless (ξ, η) coordinates.

$$N_1(\xi,\eta) = \frac{(1-\xi)(1-\eta)}{4}$$

$$N_2(\xi,\eta) = \frac{(1+\xi)(1-\eta)}{4}$$

$$N_3(\xi,\eta) = \frac{(1+\xi)(1+\eta)}{4}$$

$$N_4(\xi,\eta) = \frac{(1-\xi)(1+\eta)}{4} \tag{19.51}$$

After the element is mapped from natural to physical coordinates, the ξ and η axes need not remain orthogonal.

The principal reason for using isoparametric elements is to avoid integrating in physical coordinates. However, the general expression for the stiffness matrix, Eq. (19.31), is expressed in terms of physical coordinates. Therefore, the differential lengths dx and dy must be expressed in terms of the natural coordinate differentials $d\xi$ and $d\eta$. In addition, strain is defined in terms of the derivatives of the shape functions with respect to physical coordinates. These derivatives are the elements in the $[B]$ matrix, and they must be converted to derivatives with respect to natural coordinates.

The differentials (dx, dy) are related to the differentials $(d\xi, d\eta)$ by means of Eq. (19.49a). Thus,

$$dx = \frac{\partial x}{\partial \xi} d\xi + \frac{\partial x}{\partial \eta} d\eta$$

$$dy = \frac{\partial y}{\partial \xi} d\xi + \frac{\partial y}{\partial \eta} d\eta \tag{19.52}$$

where

$$\frac{\partial x}{\partial \xi} = \sum \frac{\partial N_i}{\partial \xi} x_i, \qquad \frac{\partial y}{\partial \xi} = \sum \frac{\partial N_i}{\partial \xi} y_i$$

$$\frac{\partial x}{\partial \eta} = \sum \frac{\partial N_i}{\partial \eta} x_i, \qquad \frac{\partial y}{\partial \eta} = \sum \frac{\partial N_i}{\partial \eta} y_i$$

The coordinate derivatives are combined in matrix form as

$$[J] = \begin{bmatrix} \dfrac{\partial x}{\partial \xi} & \dfrac{\partial y}{\partial \xi} \\ \dfrac{\partial x}{\partial \eta} & \dfrac{\partial y}{\partial \eta} \end{bmatrix} \tag{19.53}$$

where $[J]$ is the *Jacobian* of the transformation (Courant, 1950).

Equations (19.52) and (19.53) relate the differentials of the two coordinate systems as

$$\begin{Bmatrix} dx \\ dy \end{Bmatrix} = [J]^T \begin{Bmatrix} d\xi \\ d\eta \end{Bmatrix} \tag{19.54}$$

In a like manner, derivatives of the shape function for node i are related by

$$\begin{Bmatrix} \dfrac{\partial N_i}{\partial x} \\ \dfrac{\partial N_i}{\partial y} \end{Bmatrix} = [J]^{-1} \begin{Bmatrix} \dfrac{\partial N_i}{\partial \xi} \\ \dfrac{\partial N_i}{\partial \eta} \end{Bmatrix} \tag{19.55}$$

If $[J]^{-1}$ exists, then the area mapping from (ξ, η) coordinates to (x, y) coordinates is unique and reversible. A physical interpretation of $[J]$ can be obtained by comparing the area of the element in (x, y) coordinates to that in (ξ, η) coordinates. If the determinate $|J| > 0$, then the area of the element is preserved and the mapping is physically meaningful. In precise terms, $|J|$ is the differential area ratio $A_{xy}/A_{\xi\eta}$ at any point in the element.

This physical interpretation of $[J]$ leads to a change in the differential volume for a constant thickness, plane elasticity element from $t\,dx\,dy$ to $t|J|\,d\xi\,d\eta$. The limits of integration are -1 to 1 in ξ and -1 to 1 in η. So, the integral of any function $F(x, y)$ can be transformed to natural coordinates in the manner

$$\int_A F(x, y)\,dx\,dy = \int_{-1}^{1}\int_{-1}^{1} F(x(\xi, \eta), y(\xi, \eta))|J|\,d\xi\,d\eta$$

Element Stiffness Matrix

Equation (19.31) defines the element stiffness matrix for any elasticity element (using displacement DOF), including the isoparametric linear quadrilateral. A change in coordinate system from (x, y) to (ξ, η), with the modified limits of integration, leads to the stiffness matrix

$$[K] = t\int_{-1}^{1}\int_{-1}^{1} [B]^T[D][B]|J|\,d\xi\,d\eta \tag{19.56}$$

where $[B]$ is given by Eq. (19.47) and $[B_i]$ by Eq. (19.48). From Eqs. (19.48) and (19.55), the individual terms in $[B_i]$, in terms of (ξ, η), are

$$[B_i(\xi, \eta)] = \begin{bmatrix} J_{11}^* \dfrac{\partial N_i}{\partial \xi} + J_{12}^* \dfrac{\partial N_i}{\partial \eta} & 0 \\ 0 & J_{21}^* \dfrac{\partial N_i}{\partial \xi} + J_{22}^* \dfrac{\partial N_i}{\partial \eta} \\ J_{21}^* \dfrac{\partial N_i}{\partial \xi} + J_{22}^* \dfrac{\partial N_i}{\partial \eta} & J_{11}^* \dfrac{\partial N_i}{\partial \xi} + J_{12}^* \dfrac{\partial N_i}{\partial \eta} \end{bmatrix} \tag{19.57}$$

where J_{ij}^* is the i,j term from $[J]^{-1}$.

It is usually more convenient to work with just a single (2×2) nodal submatrix of $[K]$ at one time. Hence, we write

$$[K_{ij}] = t\int_{-1}^{1}\int_{-1}^{1} [B_i]^T[D][B_j]|J|\,d\xi\,d\eta \tag{19.58}$$

where i and j are node numbers for the element.

Numerical Integration

Although analytical expressions for the individual terms in Eq. (19.58) can be developed, they are quite complex and, thus, prone to errors in algebra or computer programming. As an alternative to direct integration, the required integrals are usually evaluated numerically within the finite element program. The most commonly used numerical integration method is *Gauss quadrature*. The Gauss quadrature method is more efficient than many other methods, such as the Newton–Cotes methods, since fewer sampling points are required to obtain a given level of accuracy. In fact, in one dimension, the use of n sampling points in Gauss quadrature results in exact integration of a polynomial of order $(2n - 1)$. However, the integration of a function that is not a polynomial is approximate.

Consider a function $F(\xi, \eta)$ that is to be integrated over the limits of -1 to 1 in ξ and -1 to 1 in η. The integral is evaluated numerically by the form

$$I = \int_{-1}^{1} \int_{-1}^{1} F(\xi, \eta)\, d\xi\, d\eta = \sum_{k=1}^{m} \sum_{l=1}^{n} w_k w_l F(\xi_k, \eta_l)$$

where m and n are the numbers of sampling points in the ξ and η directions, respectively. Also, ξ_k and η_l are the locations of the kth and lth sampling points and w_k and w_l are weights applied to $F(\xi, \eta)$ after it is evaluated at the sampling points. Usually, m and n are taken as equal, in which case the numerical scheme is symmetric.

If Gauss quadrature is used to evaluate the nodal submatrix $[K_{ij}]$ in Eq. (19.58), the integral becomes

$$[K_{ij}] = t \sum_{k=1}^{m} \sum_{l=1}^{n} w_k w_l [B_i(\xi_k, \eta_l)]^T [D] [B_j(\xi_k, \eta_l)] |J(\xi_k, \eta_l)| \qquad (19.59)$$

The accuracy achieved with Gauss quadrature is dependent on the proper selection of sampling point locations and weights. For elements in natural coordinates, the optimal sampling point locations and weights are given in Fig. 19.10. Only symmetric integration and the one-, two-, and three-point rules are considered. Nonsymmetric integration and higher-order integration rules are discussed elsewhere.

The number of integration points used to evaluate Eq. (19.59) influences the ultimate performance of the element. *Full integration* is the integration order needed to *exactly* integrate the stiffness for an undistorted element. For the linear quadrilateral, a two-point rule provides full integration. An integration rule less than that required for full integration is termed *reduced integration*. Reduced integration, although not exactly evaluating Eq. (19.59), can often lead to improved performance of an element, relative to full integration. For instance, reduced integration of the linear quadrilateral can eliminate the parasitic shear that is a common defect in the element (see Example 19.3). A more complete discussion of reduced integration, including justification for its use, can be found in most finite element textbooks.

High-Order Isoparametric Elements

The concept of isoparametric mapping has been applied to a broad list of element geometries. Within the scope of plane elasticity problems, elements with more than four nodes permit greater flexibility in element shape (including curved edges) and

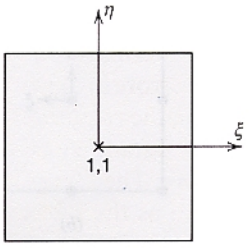

Point No.	ξ_i	η_j	w_i	w_j
1,1	0.0	0.0	1.0	1.0

(*a*)

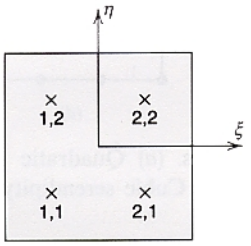

Point No.	ξ_i	η_j	w_i	w_j
1,1	$-1/\sqrt{3}$	$-1/\sqrt{3}$	1.0	1.0
2,1	$1/\sqrt{3}$	$-1/\sqrt{3}$	1.0	1.0
1,2	$-1/\sqrt{3}$	$1/\sqrt{3}$	1.0	1.0
2,2	$1/\sqrt{3}$	$1/\sqrt{3}$	1.0	1.0

(*b*)

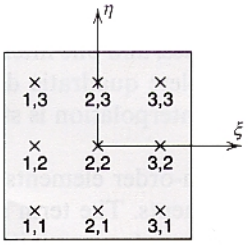

Point No.	ξ_i	η_j	w_i	w_j
1,1	$-\sqrt{0.6}$	$-\sqrt{0.6}$	5/9	5/9
2,1	0	$-\sqrt{0.6}$	8/9	5/9
3,1	$\sqrt{0.6}$	$-\sqrt{0.6}$	5/9	5/9
1,2	$-\sqrt{0.6}$	0	5/9	8/9
2,2	0	0	8/9	8/9
3,2	$\sqrt{0.6}$	0	5/9	8/9
1,3	$-\sqrt{0.6}$	$\sqrt{0.6}$	5/9	5/9
2,3	0	$\sqrt{0.6}$	8/9	5/9
3,3	$\sqrt{0.6}$	$\sqrt{0.6}$	5/9	5/9

(*c*)

Figure 19.10 Optimal sampling point locations and weights for Gauss quadrature. (*a*) One-point rule. (*b*) Two-point rule. (*c*) Three-point rule.

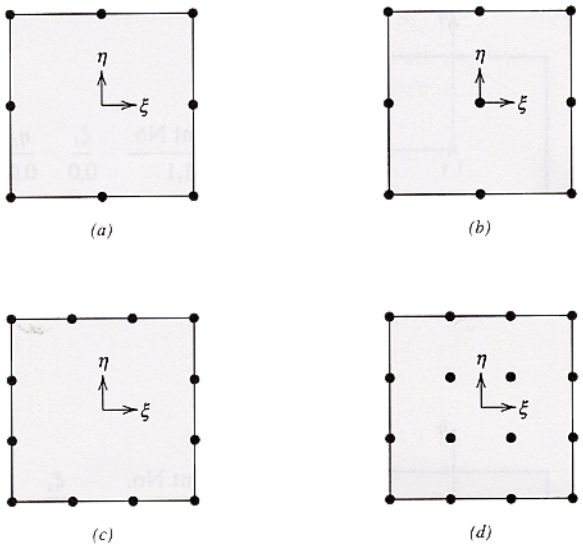

Figure 19.11 Higher-order isoparametric elements. (*a*) Quadratic serendipity element. (*b*) Quadratic Lagrange element. (*c*) Cubic serendipity element. (*d*) Cubic Lagrange element.

are capable of representing greater variation in displacements. Perhaps the most popular of all isoparametric elements is the eight-node quadrilateral. This element has four corner nodes, like the linear quadrilateral, but it also has four midside nodes, one midway along the length of each edge, (Fig. 19.11*a*.). With three nodes along each edge, the element can have curved (parabolic) sides. Another popular high-order isoparametric element is the nine-node quadrilateral (Fig. 19.11*b*.) This element has four corner nodes, four midside nodes, and one interior node. Both the eight- and nine-node elements represent complete quadratic displacement fields. The generalization of these elements to cubic interpolation is straightforward, see Figs. 19.11*c* and *d*.

The eight-node quadrilateral and other high-order elements that contain only boundary nodes are known as *serendipity* elements. The term serendipity is used because shape functions for this family of elements were initially developed by inspection. The nine-node quadrilateral and other high-order elements that contain a regular pattern of nodes are known as Lagrangian elements since their shape functions are based on the Lagrange interpolation functions.

19.5 THE PLANE FRAME ELEMENT

Analysis of framed structures by the *stiffness method* (also known as *matrix analysis*) was fairly well established at the time of the development of the finite element method. The stiffness method for frame analysis can be developed entirely from basic mechanics of material principles, without the need to consider virtual work

formulations and interpolation polynomials. As a result, many engineers view the two methods as distinct. However, it is clear that the stiffness method for frames is simply a special case of the finite element method. Hence, in this section, we develop a finite element that represents a plane frame member, using the same approach that was used for plane elasticity problems.

Element Stiffness Matrix

The classical plane frame element has two nodes, it is straight and prismatic, and it has three DOF and three corresponding end actions at each node (see Fig. 19.12*a*). The element has constant cross-sectional area A, moment of inertia I, and modulus of elasticity E. We assume that the axial response of the member is independent of the bending response. Consequently, the frame element stiffness is formulated as a superposition of the stiffness for an axial rod and that for a beam (Fig. 19.12*b*). In the following, a *local* $(\bar{x}, \bar{y})$ coordinate system is established for the element. The local $\bar{x}$ axis is aligned with the longitudinal axis of the member, and the $\bar{y}$ axis lies in the plane of the element cross section. The stiffness matrix for the frame element is derived in terms of this local coordinate system. When the element is oriented at some angle ϕ with respect to the *global* (x, y) coordinates for the structure, the nodal DOF of the element must be related to the global coordinate system. Thus, a coordinate rotation from local to global coordinates is required for the displacements, loads, and stiffness. This rotation is discussed following Eq. (19.75).

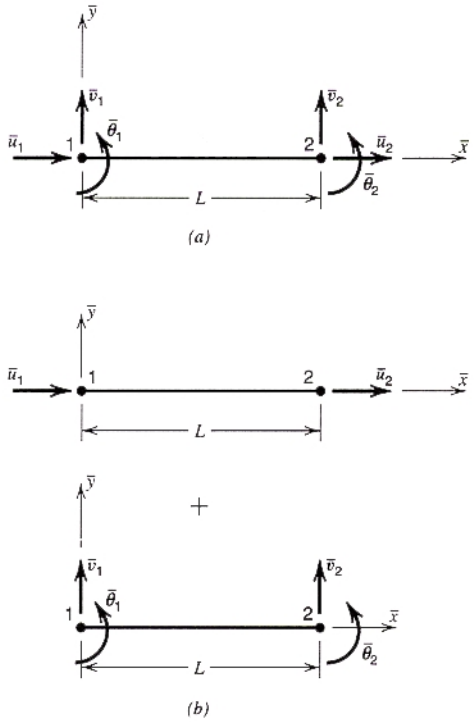

Figure 19.12 Plane frame element. (*a*) Element with combined axial and bending DOF. (*b*) Axial and bending DOF treated separately.

Consider first the case of the axial rod. There are two nodal DOF associated with axial response, so the displacement is taken as a linear function

$$\bar{u}(x) = a_0 + a_1 \bar{x}$$

The coefficients a_0 and a_1 are evaluated based on the boundary conditions $\bar{u}(0) = \bar{u}_1$ and $\bar{u}(L) = \bar{u}_2$, where L is the element length. The displacement function, in terms of the nodal displacements, becomes

$$\bar{u}\,(x) = [N]\{\bar{u}_i\}$$

where $[N] = [1 - \bar{x}/L \quad \bar{x}/L]$ and $\{\bar{u}_i\} = [\bar{u}_1 \quad \bar{u}_2]^T$.

The only nonzero strain component is ϵ_{xx}, which is written in terms of the nodal displacements as

$$\epsilon_{xx} = [B_A]\{\bar{u}_i\}$$

in which the subscript A indicates *axial* response and

$$[B_A] = \left[\frac{\partial N_1}{\partial \bar{x}} \quad \frac{\partial N_2}{\partial \bar{x}}\right] = \left[-\frac{1}{L} \quad \frac{1}{L}\right]$$

The axial stress is written as $\sigma_{xx} = E\epsilon_{xx}$ and the variation of internal energy is

$$\delta U = \int_V \delta\epsilon_{xx}\sigma_{xx}\, dV \tag{19.60}$$

Assume that only concentrated nodal loads are applied. Substitution for σ_{xx} and $\delta\epsilon_{xx}$ in Eq. (19.60), and then substitution of Eq. (19.60) into Eq. (19.1), yield

$$\{\delta\bar{u}_i\}^T\{\bar{F}_i\} - \{\delta\bar{u}_i\}^T\left[A\int_0^L [B_A]^T E[B_A]\, d\bar{x}\right]\{\bar{u}_i\} = 0$$

Since $\{\delta\bar{u}_i\}$ is arbitrary,

$$\{\bar{F}_i\} = \left[A\int_0^L [B_A]^T E[B_A]\, d\bar{x}\right]\{\bar{u}_i\}$$

which leads to the stiffness matrix for the axial rod

$$[\bar{K}_A] = A\int_0^L [B_A]^T E[B_A]\, d\bar{x}$$

For constant E, the integrals are easily evaluated to obtain $[\bar{K}_A]$ in terms of A, E, and L.

$$[\bar{K}_A] = \left[\begin{array}{c|c} \dfrac{AE}{L} & -\dfrac{AE}{L} \\ \hline -\dfrac{AE}{L} & \dfrac{AE}{L} \end{array}\right] \tag{19.61}$$

Next consider the *bending* effect of the frame element. There are four nodal DOF associated with bending (a lateral translation and a rotation at each node), so the displacement is written as a cubic polynomial with four coefficients.

$$\bar{v}(x) = a_0 + a_1\bar{x} + a_2\bar{x}^2 + a_3\bar{x}^3$$

The coefficients a_0 through a_3 are evaluated based on the boundary conditions $\bar{v}(0) = \bar{v}_1$, $\bar{\theta}(0) = \bar{\theta}_1$, $\bar{v}(L) = \bar{v}_2$, and $\bar{\theta}(L) = \bar{\theta}_2$ in which $\bar{\theta} = d\bar{v}/d\bar{x}$. In terms of the of the nodal displacements, the displacement function is

$$\bar{v}(\bar{x}) = [N]\{\bar{v}_i\} \tag{19.62}$$

where $\{\bar{v}_i\} = [\bar{v}_1 \quad \bar{\theta}_1 \quad \bar{v}_2 \quad \bar{\theta}_2]^T$, and the shape function matrix $[N]$ is

$$[N] = [N_1 \quad N_2 \quad N_3 \quad N_4] \tag{19.63a}$$

for which the individual shape functions are

$$\begin{aligned} N_1 &= 1 - 3\frac{\bar{x}^2}{L^2} + 2\frac{\bar{x}^3}{L^3} \\ N_2 &= \bar{x} - 2\frac{\bar{x}^2}{L} + \frac{\bar{x}^3}{L^2} \\ N_3 &= 3\frac{\bar{x}^2}{L^2} - 2\frac{\bar{x}^3}{L^3} \\ N_4 &= -\frac{\bar{x}^2}{L} + \frac{\bar{x}^3}{L^2} \end{aligned} \tag{19.63b}$$

These shape functions are illustrated in Fig. 19.13.

The strain energy in a beam subjected to bending is given by Eq. (5.19); that is,

$$U = \int_0^L \frac{M^2}{2EI}\,d\bar{x} \tag{5.19}$$

If the curvature $\bar{v}''$ is taken as a *generalized strain* quantity, the strain-nodal displacement relation is

$$\bar{v}''(\bar{x}) = [B_B]\{\bar{v}_i\} \tag{19.64a}$$

where the subscript B represents *bending* response and

$$[B_B] = \left[\frac{d^2N_1}{d\bar{x}^2} \quad \frac{d^2N_2}{d\bar{x}^2} \quad \frac{d^2N_3}{d\bar{x}^2} \quad \frac{d^2N_4}{d\bar{x}^2}\right] \tag{19.64b}$$

Substitution of $M = EI\bar{v}''$ into Eq. (5.19) gives

$$U = \int_0^L \frac{EI(\bar{v}'')^2}{2}\,d\bar{x} \tag{19.65}$$

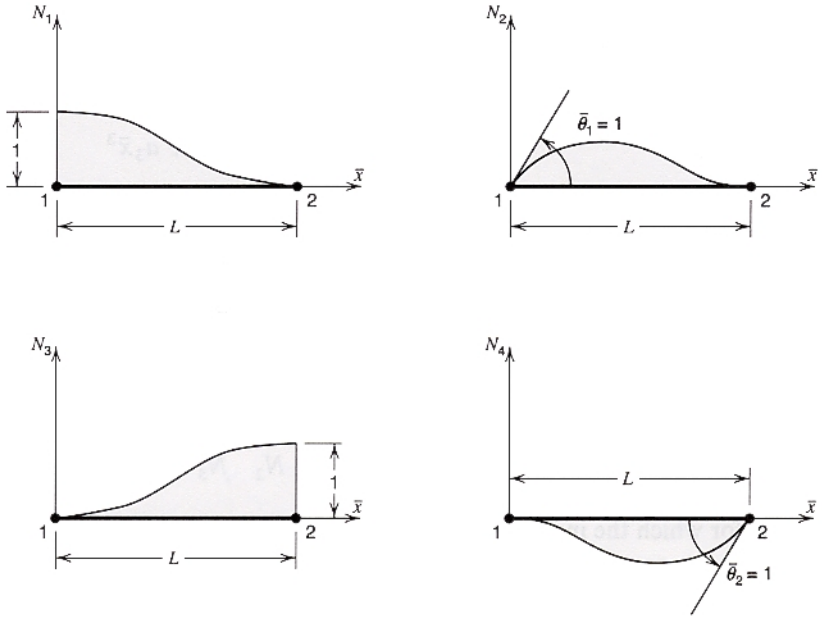

Figure 19.13 Beam element shape functions.

from which the first variation of the strain energy is

$$\delta U = \int_0^L (\delta \bar{v})'' EI \bar{v}'' \, d\bar{x}$$

In terms of nodal DOF, from Eq. (19.64a), δU is

$$\delta U = \int_0^L \{\delta \bar{v}_i\}^T [B_B]^T EI [B_B] \{\bar{v}_i\} \, d\bar{x} \tag{19.66}$$

In the manner followed with other elements, only nodal loads are assumed, Eq. (19.66) is substituted into Eq. (19.1), $\{\delta v_i\}$ is eliminated, and the bending stiffness matrix is found to be

$$[\bar{K}_B] = \int_0^L [B_B]^T EI [B_B] \, d\bar{x}$$

Since EI is constant, integration yields the bending stiffness matrix in terms of E, I, and L as

$$[\bar{K}_B] = \left[\begin{array}{cc:cc} \frac{12EI}{L^3} & \frac{6EI}{L^2} & \frac{-12EI}{L^3} & \frac{6EI}{L^2} \\ \frac{6EI}{L^2} & \frac{4EI}{L} & \frac{-6EI}{L^2} & \frac{2EI}{L} \\ \hdashline \frac{-12EI}{L^3} & \frac{-6EI}{L^2} & \frac{12EI}{L^3} & \frac{-6EI}{L^2} \\ \frac{6EI}{L^2} & \frac{2EI}{L} & \frac{-6EI}{L^2} & \frac{4EI}{L} \end{array}\right] \tag{19.67}$$

The stiffness matrix for the plane frame element [see Eq. (19.68)] is a combination of the axial stiffness matrix, Eq. (19.61), and the bending stiffness matrix, Eq. (19.67). Note that the ordering of the DOF in the element first lists all three DOF at node 1 and then the three DOF at node 2.

$$[\bar{K}] = \left[\begin{array}{ccc:ccc} \frac{AE}{L} & 0 & 0 & \frac{-AE}{L} & 0 & 0 \\ 0 & \frac{12EI}{L^3} & \frac{6EI}{L^2} & 0 & \frac{-12EI}{L^3} & \frac{6EI}{L^2} \\ 0 & \frac{6EI}{L^2} & \frac{4EI}{L} & 0 & \frac{-6EI}{L^2} & \frac{2EI}{L} \\ \hdashline \frac{-AE}{L} & 0 & 0 & \frac{AE}{L} & 0 & 0 \\ 0 & \frac{-12EI}{L^3} & \frac{-6EI}{L^2} & 0 & \frac{12EI}{L^3} & \frac{-6EI}{L^2} \\ 0 & \frac{6EI}{L^2} & \frac{2EI}{L} & 0 & \frac{-6EI}{L^2} & \frac{4EI}{L} \end{array}\right] \tag{19.68}$$

The displacement vector $\{\bar{u}_i\}$ for the element is

$$\{\bar{u}_i\} = [\bar{u}_1 \quad \bar{v}_1 \quad \bar{\theta}_1 \quad \bar{u}_2 \quad \bar{v}_2 \quad \bar{\theta}_2]^T \tag{19.69}$$

and the element end action (load) vector $\{\bar{P}_i\}$ is

$$\{\bar{P}_i\} = [\bar{P}_{x1} \quad \bar{P}_{y1} \quad \bar{M}_1 \quad \bar{P}_{x2} \quad \bar{P}_{y2} \quad \bar{M}_2]^T \tag{19.70}$$

Finally, the relationship between nodal loads and nodal displacements for an element in local coordinates is given by the familiar form

$$[\bar{K}]\{\bar{u}_i\} = \{\bar{P}_i\} \tag{19.71}$$

Equivalent Nodal Load Vector

As for most other elements, actual loads that are applied over the element must be converted to equivalent nodal loads. We consider only element loads that affect beam behavior. Two cases are considered: a distributed load over a portion of the element and a transverse concentrated force. Equivalent nodal loads for axial behavior are derived in a like fashion.

For a distributed load along the beam, not necessarily over the full length, the variation of work δW_D of the load is

$$\delta W_D = \int_{L_a}^{L_b} \delta\bar{v}\bar{q}(\bar{x})\, d\bar{x} \tag{19.72}$$

where $\bar{q}(\bar{x})$ is the load function that exists over the domain $L_a < \bar{x} < L_b$ (see Fig. 19.14*a*) and the subscript D denotes a distributed load. Equation (19.62) is substituted into Eq. (19.72), and the equivalent nodal load vector is obtained as

$$\{\bar{P}_{Di}\} = \int_{L_a}^{L_b} [N]^T \bar{q}(\bar{x})\, d\bar{x} \tag{19.73}$$

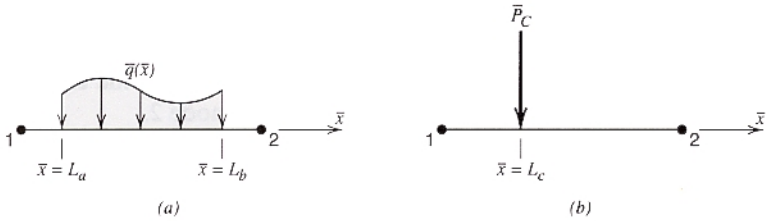

Figure 19.14 Element loads for beam element. (*a*) Distributed load. (*b*) Concentrated load.

For a concentrated load $\bar{P}_C$ located at $\bar{x} = L_c$ along the beam (see Fig. 19.14*b*) the variation of work δW_C of the load is

$$\delta W_C = \delta \bar{v}|_{\bar{x}=L_c} \bar{P}_C \tag{19.74}$$

The variation of displacement $\delta \bar{v}$ at $\bar{x} = L_c$ is written in terms of the variation of nodal displacements by Eq. (19.62) with the shape functions evaluated at $\bar{x} = L_c$. The equivalent nodal load vector is

$$\{\bar{P}_{Ci}\} = [N]|^T_{\bar{x}=L_c} \bar{P}_C \tag{19.75}$$

By Eqs. (19.73) and (19.75), equivalent nodal load vectors for several load patterns on a beam element were determined and are shown in Fig. 19.15.

Coordinate Rotations

Consider an element in a structure oriented at an angle ϕ with respect to the global x axis (Fig. 19.16). To assemble the stiffness matrix and load vector for this element with those of other elements, all nodal DOF must be defined in terms of the global coordinate system. For node i, the displacements in the two coordinate systems are related by

$$\begin{Bmatrix} \bar{u}_i \\ \bar{v}_i \\ \bar{\theta}_i \end{Bmatrix} = [\lambda] \begin{Bmatrix} u_i \\ v_i \\ \theta_i \end{Bmatrix} \tag{19.76}$$

where

$$[\lambda] = \begin{bmatrix} \cos\phi & \sin\phi & 0 \\ -\sin\phi & \cos\phi & 0 \\ 0 & 0 & 1 \end{bmatrix}$$

For a plane frame element, with two nodes, the displacements are related by

$$\{\bar{u}_i\} = [T]\{u_i\} \tag{19.77}$$

where the rotation (transformation) matrix $[T]$ is

$$[T] = \left[\begin{array}{c|c} \lambda & 0 \\ \hline 0 & \lambda \end{array}\right]$$

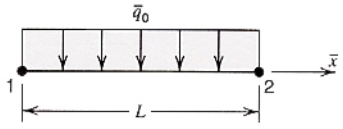

$$\{\bar{P}_{Di}\} = \begin{Bmatrix} -\dfrac{\bar{q}_0 L}{2} \\ -\dfrac{\bar{q}_0 L^2}{12} \\ \hline -\dfrac{\bar{q}_0 L}{2} \\ \dfrac{\bar{q}_0 L^2}{12} \end{Bmatrix}$$

(a)

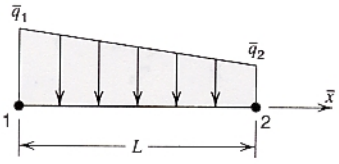

$$\{\bar{P}_{Di}\} = \begin{Bmatrix} -\dfrac{L}{20}(7\bar{q}_1 + 3\bar{q}_2) \\ -\dfrac{L^2}{60}(3\bar{q}_1 + 2\bar{q}_2) \\ \hline -\dfrac{L}{60}(3\bar{q}_1 + 7\bar{q}_2) \\ \dfrac{L^2}{60}(2\bar{q}_1 + 3\bar{q}_2) \end{Bmatrix}$$

(b)

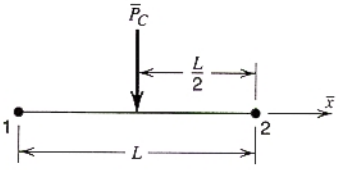

$$\{\bar{P}_{Ci}\} = \begin{Bmatrix} -\dfrac{\bar{P}_C}{2} \\ -\dfrac{\bar{P}_C L}{8} \\ \hline -\dfrac{\bar{P}_C}{2} \\ \dfrac{\bar{P}_C L}{8} \end{Bmatrix}$$

(c)

Figure 19.15 Equivalent nodal loads for beam element. (*a*) Uniformly distributed load. (*b*) Linearly distributed load. (*c*) Concentrated load.

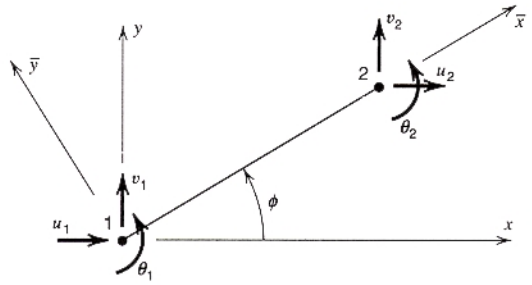

Figure 19.16 Frame element in global coordinates.

TABLE 19.4
Element Stiffness Matrix for Plane Frame Element in Global Coordinates

column index $j \rightarrow$ 1 2 3 4 5 6 row index $i \downarrow$

$$[K] = \left[\begin{array}{cccccc|l}
c^2\frac{AE}{L} + s^2\frac{12EI}{L^3} & sc\left(\frac{AE}{L} - \frac{12EI}{L^3}\right) & -s\left(\frac{6EI}{L^2}\right) & -c^2\frac{AE}{L} - s^2\frac{12EI}{L^3} & -sc\left(\frac{AE}{L} - \frac{12EI}{L^3}\right) & -s\left(\frac{6EI}{L^2}\right) & 1 \\
sc\left(\frac{AE}{L} - \frac{12EI}{L^3}\right) & s^2\frac{AE}{L} + c^2\frac{12EI}{L^3} & c\left(\frac{6EI}{L^2}\right) & -sc\left(\frac{AE}{L} - \frac{12EI}{L^3}\right) & -s^2\frac{AE}{L} - c^2\frac{12EI}{L^3} & c\left(\frac{6EI}{L^2}\right) & 2 \\
-s\left(\frac{6EI}{L^2}\right) & c\left(\frac{6EI}{L^2}\right) & \frac{4EI}{L} & s\left(\frac{6EI}{L^2}\right) & -c\left(\frac{6EI}{L^2}\right) & \frac{2EI}{L} & 3 \\
\hline
-c^2\frac{AE}{L} - s^2\frac{12EI}{L^3} & -sc\left(\frac{AE}{L} - \frac{12EI}{L^3}\right) & s\left(\frac{6EI}{L^2}\right) & c^2\frac{AE}{L} + s^2\frac{12EI}{L^3} & sc\left(\frac{AE}{L} - \frac{12EI}{L^3}\right) & s\left(\frac{6EI}{L^2}\right) & 4 \\
-sc\left(\frac{AE}{L} - \frac{12EI}{L^3}\right) & -s^2\frac{AE}{L} - c^2\frac{12EI}{L^3} & -c\left(\frac{6EI}{L^2}\right) & sc\left(\frac{AE}{L} - \frac{12EI}{L^3}\right) & s^2\frac{AE}{L} + c^2\frac{12EI}{L^3} & -c\left(\frac{6EI}{L^2}\right) & 5 \\
-s\left(\frac{6EI}{L^2}\right) & c\left(\frac{6EI}{L^2}\right) & \frac{2EI}{L} & s\left(\frac{6EI}{L^2}\right) & -c\left(\frac{6EI}{L^2}\right) & \frac{4EI}{L} & 6
\end{array}\right]$$

$c = \cos\phi, \qquad s = \sin\phi$

In like manner, element end actions (loads) are rotated by

$$\{\bar{P}_i\} = [T]\{P_i\} \tag{19.78}$$

Substitution of Eqs. (19.77) and (19.78) into Eq. (19.71) yields

$$[\bar{K}][T]\{u_i\} = [T]\{P_i\} \tag{19.79}$$

Premultipling both sides of Eq. (19.79) by $[T]^{-1}$ and observing that $[T]^{-1} = [T]^T$, since $[T]$ is an orthogonal matrix, we obtain

$$[T]^T[\bar{K}][T]\{u_i\} = \{P_i\}$$

Thus, since $\{u_i\}$ and $\{P_i\}$ are in global coordinates, the stiffness matrix for the plane frame element, in global coordinates, is

$$[K] = [T]^T[\bar{K}][T] \tag{19.80}$$

The final form of $[K]$ is given in Table 19.4. The load vector for the element, in global coordinates, is obtained from Eq. (19.78) as

$$\{P_i\} = [T]^T\{\bar{P}_i\} \tag{19.81}$$

19.6 CLOSING REMARKS

Requirements for Accuracy

The accuracy of a finite element solution strongly depends on two conditions. First, it is important that the equations of equilibrium be satisfied throughout the model. Second, it is also important that compatibility (continuity of displacements) be maintained. In certain circumstances, these conditions are violated, as noted below.

Equilibrium at the structure nodes is satisfied since the basic system of equations, Eq. (19.45), is fundamentally a system of nodal equilibrium equations. Thus, within the accuracy of the equation-solving process (numerical error), the structure nodes are in equilibrium.

For elements with only displacement DOF, equilibrium along element edges is generally *not* satisfied. This is because although displacements might be continuous across element boundaries, their derivatives are not, and thus, stresses are not continuous. For instance, consider two constant strain triangle elements, such as those shown in Fig. 19.17. Nodes 1, 2, and 3 are fully constrained, whereas node 4 has an imposed displacement in the x direction. Hence, element 1 is unstressed, whereas element 2 has nonzero σ_{xx}. Because of the stress discontinuity, a differential element located at the boundary between the two elements does not satisfy equilibrium in the x direction.

Equilibrium within an element is *not* satisfied, unless body forces are of relatively low order or are entirely absent. For a constant strain triangle, the stress

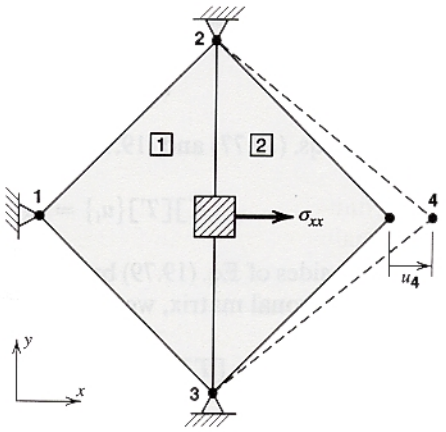

Figure 19.17 Equilibrium along element edges.

state is constant throughout the element. Thus, equilibrium of a differential element is satisfied only when body forces are absent [see Eq. (2.45)]. Similarly, for elements that can represent linear stress variation, body forces must be, at most, constant in magnitude for equilibrium.

Compatibility at the nodes is assured because of the assembly process. That is, the displacements of adjacent elements are the same at their common nodes. However, to assure that compatibility is maintained along the common edge between two adjacent elements, the displacements along that edge, viewed from either element, must be expressed entirely in terms of the displacement of nodes on that edge. Elements that maintain compatibility along common edges are known as *conforming* elements. Generally, this condition is satisfied for elements that possess only translational DOF. However, certain plate-bending and shell elements, for instance, are nonconforming.

Compatibility within an element is assured so long as the displacement interpolation polynomials are continuous.

Requirements for Convergence

As discussed at the beginning of this chapter, a major source of error in a finite element solution is the use of approximation functions to describe element response (formulation error). To reduce formulation error, we successively refine our finite element models with the expectation that the numerical solution will converge to the *exact* solution. Under certain conditions, convergence can be guaranteed. These conditions are the following:

1. The elements must be complete. That is, the shape function must be a complete polynomial. For instance, a complete quadratic contains all possible quadratic terms and omits no linear or constant terms. Inclusion of a few cubic terms, such as for the quadratic serendipity and Lagrange elements, does not destroy completeness of the quadratic polynomial.
2. The elements must be compatible. Hence, continuity of displacements must be assured throughout the entire structural model.

3. The elements must be capable of representing rigid-body motion and constant strain. For two- and three-dimensional elasticity problems, these are assured if the displacement field contains at least a complete linear polynomial. For shell elements, constant strain implies constant curvature and constant twist [see Eq. (13.30)]. Some shell elements cannot represent rigid-body motion.

Generally, a finite element model is too stiff. That is, displacements converge from below. A qualitative explanation is as follows. The elements are *constrained*, by the shape functions, to deform in a specific (unnatural) manner. This constraint adds stiffness, relative to the physical system, that results in smaller displacements when the external influences on the system are loads. If all external loads are zero and the only external influences on the system are imposed (nonzero) displacements, additional energy is required to force the model into the imposed deformed shape.

For isoparametric elements, reduced integration can be used effectively to *soften* the element such that its response improves relative to full integration. Problem 19.1 demonstrates how the use of approximation functions to represent displacements results in a model that is stiff relative to the actual system.

Modeling Recommendations

As an aid to the application of the finite-element method to analysis of practical problems in elasticity, the following recommendations are offered. The list is not exhaustive and the recommendations themselves are not rigid rules that cannot be violated.

1. Avoid abrupt transitions in element size and geometry. Limit the change in *element stiffness* (approximated by E/V_e, where V_e is the volume of the element) from one element to the next to roughly a factor of 3.
2. Avoid unnecessary element irregularity. Keep aspect ratios (the length ratio of the longest side to the shortest side) less than 10:1. Interior angles of quadrilaterals should be as regular as possible. They should not exceed 150° and they should not be less than 30°. Midside nodes on quadratic elements should be within the middle third of the edge.
3. Maintain compatibility between elements. For instance, it is not appropriate to attach one quadratic quadrilateral to two linear quadrilaterals simply because they have three nodes in common. Such an assembly would not maintain compatibility because of the difference in displacement interpolation on the two sides of the boundary; see Fig. 19.18.

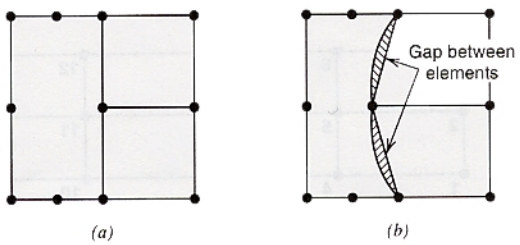

Figure 19.18 Assembly of incompatible elements. (*a*) Undistorted assembly. (*b*) Loss of compatibility under distortion.

4. Use a fine mesh in regions of high stress gradient (stress concentration); use a coarse mesh where gradients are low.
5. When Choleski decomposition, or any other *band* solver, is used, minimize the bandwidth of the assembled structure stiffness matrix by proper node numbering. The nonzero entries in the structure stiffness matrix are clustered about the diagonal in a band. The *bandwidth* is the number of terms across a row (or down a column) of the band. The *half-bandwidth* is the number of terms from the diagonal out to the edge of the band. The nodal half-bandwidth is computed as $(n_{\max} - n_{\min} + 1)$, where $n_{\max}$ and $n_{\min}$ are the largest and smallest structure node numbers in the incidence list for an element. Hence, to minimize bandwidth, keep the range of node numbers that define the incidences for a single element as small as possible. Examples of poor and good node numbering schemes are illustrated in Fig. 19.19.
6. Exploit symmetry in the geometry and loads of the physical system to build the smallest reasonable model.

The finite element method and its use in engineering practice are evolving continuously. For instance, not long ago, material and/or geometric nonlinear analyses were rarely attempted. Today, such analyses are not limited to research but are performed by practicing engineers as well. The popularity of the finite element method is due primarily to the greater availability, and affordability, of user-friendly software that integrates sophisticated analysis capabilities with solid modeling and computer-aided design (CAD). Unfortunately, user training and experience are not always equal to the capabilities of the software. Hence, the danger exists that these powerful analytical tools will be used as *black boxes*, without proper understanding of the physical system or algorithms used in the analysis. There is no substitute for common sense and sound judgment, and one should remain skeptical of computer-generated results until they can be verified by some other means.

An effective means for an engineer to gain experience in performing finite element analysis and develop confidence in a finite element program is to solve a series of relatively simple *benchmark* problems. Such problems are specially designed to

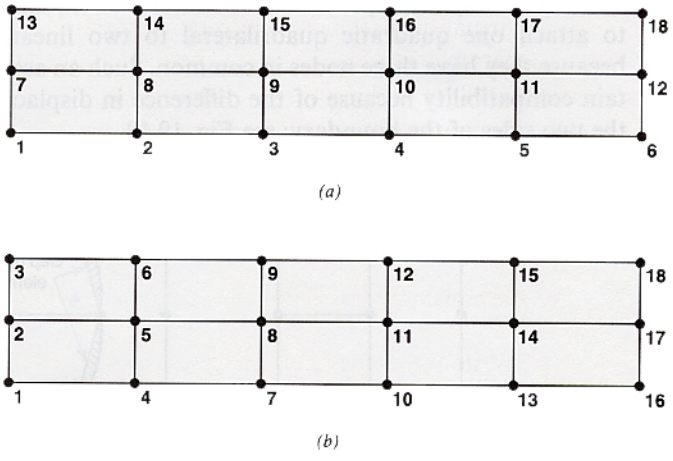

Figure 19.19 Node numbering to minimize bandwidth. (*a*) Poor numbering scheme, half-bandwidth = 8. (*b*) Good numbering scheme, half-bandwidth = 5.

test the accuracy of the individual elements in the program. However, they can also be used as a training device for novice users. A reasonable set of benchmark problems has been proposed by MacNeal and Harder (1984, 1985). Additional problems can be found in (AIAA, 1985).

PROBLEMS
Section 19.2

19.1. A transverse load P is applied to the end of a cantilever beam (Fig. P19.1). The beam has length L, moment of inertia I, and modulus of elasticity E. The displaced shape of the beam is assumed to be of the following forms:

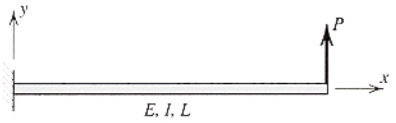

Figure P19.1

i. $v(x) = a_0 + a_1 x + a_2 x^2$

ii. $v(x) = b\left(1 - \cos\dfrac{\pi x}{2l}\right)$

iii. $v(x) = c_0 + c_1 x + c_2 x^2 + c_3 x^3$

Consider only strain energy due to bending as given by Eq. (19.65) and the potential of the load $[\Omega = -Pv(L)]$ with respect to the undeformed beam.

(a) To the extent possible, simplify each of the assumed displaced shapes to account for the boundary conditions.

(b) Calculate the elastic strain energy U and potential Ω of the external load P for each of the assumed displaced shapes.

(c) Solve for the parameters $(a_0, \ldots, c_3)$ using the principle of stationary potential energy, where for equilibrium $\delta\Pi = \delta U + \delta\Omega = 0$. *Hint*: The virtual displacement δv is first written in terms of a variation in the parameters $(\delta a_0, \ldots, \delta c_3)$. Then simultaneous equations are written from $\delta\Pi = (\partial\Pi/\partial a_0)\delta a_0 + \cdots = 0$.

(d) Compute values of Π and $v(L)$ for each of the assumed displaced shapes. Compare the values of $v(L)$ to each other and to the elasticity solution of $v(L) = (PL^3/3EI$.

(e) Discuss the results.

19.2. For the constant strain triangle element shown in Fig. P19.2

(a) Write the shape function for each node.

(b) Evaluate each shape function at point P.

(c) Show, numerically for each shape function, that the value of the shape function for node i is equal to the ratio A_{Pjk}/A_{ijk}, where A_{Pjk} is the area of triangle Pjk and A_{ijk} the area of the element.

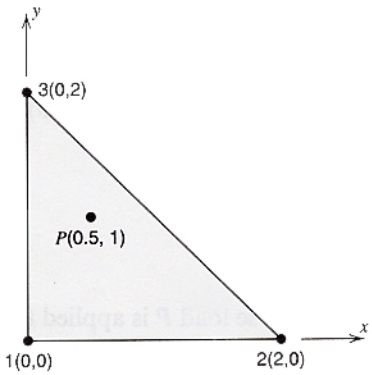

Figure P19.2

19.3. For the mesh shown in Fig. 19.5, construct the boolean connectivity matrix $[M]$ for elements 2, 3, and 4. Refer to Example 19.2.

19.4. For the mesh shown in Fig. 19.5, assemble the complete stiffness matrix for the structure. Use the notation k_{ij}^e to represent each stiffness coefficient, where the superscript identifies the element number. Refer to Example 19.2.

Section 19.4

19.5. A four-node isoparametric element has nodes at the following (x, y) coordinates: 1(0,0), 2(1,0), 3(2,2), 4(0,1).

(a) Sketch to scale the element and the lines for which $\xi = \pm\frac{1}{2}$, $\xi = \pm\frac{1}{4}$, $\eta = \pm\frac{1}{2}$, and $\eta = \pm\frac{1}{4}$.

(b) Write the coordinate interpolation functions

$$x(\xi,\eta) = \sum_{i=1}^{4} N_i(\xi,\eta)x_i \qquad \text{and} \qquad y(\xi,\eta) = \sum_{i=1}^{4} N_i(\xi,\eta)y_i.$$

(c) Compute the terms in the Jacobian matrix $[J]$ given by Eq. (19.53).

(d) Evaluate the determinate $|J|$ at $\xi = 0$, $\eta = 0$. Compare this value to the ratio of the area of the element in (x, y) coordinates to that in (ξ, η) coordinates.

19.6. For the linear isoparametric element shown in Fig. P19.6, compute $[B_1]$ at the point $\xi = 0$, $\eta = 0$.

19.7. Using the one-, two-, and three-point Gauss quadrature rules, numerically evaluate the following integrals. Compare the numerical results to the exact solutions.

(a) $I = \int_{-1}^{1} (6x^3 - 4x^2 + 3x - 2)\,dx$

(b) $I = \int_{-1}^{1} \cosh\xi\,d\xi$

(c) $I = \int_{-1}^{1} e^{\xi}\,d\xi$

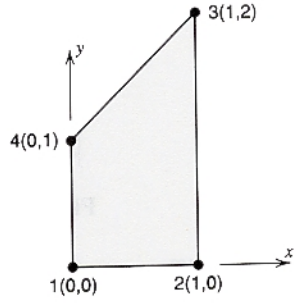

Figure P19.6

19.8. Using the one-, two-, and three-point symmetric Gauss quadrature rules, numerically evaluate the following integrals. Compare the numerical results to the exact solutions.

(a) $I = \int_{-1}^{1}\int_{-1}^{1} \cos\xi \cos\eta \, d\xi \, d\eta$

(b) $I = \int_{-1}^{1}\int_{-1}^{1} \sin^2\xi \cos\eta \, d\xi \, d\eta$

Section 19.5

19.9. Derive the equivalent nodal load vector for an axial rod element subjected to a concentrated axial force $\bar{P}_C$ acting at L_c from node 1, see Fig. P19.9.

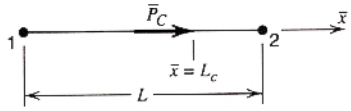

Figure P19.9

19.10. Derive the equivalent nodal load vector for an axial rod subjected to a uniformly distributed axial force of magnitude $\bar{q}_0$ acting over the domain $L_a < \bar{x} < L_b$, see Fig. P19.10

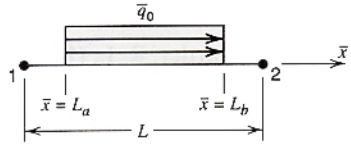

Figure P19.10

19.11. Derive the equivalent nodal load vector for a beam element subjected to a concentrated bending moment $\bar{M}_C$ acting at L_c from node 1; see Fig. P19.11.

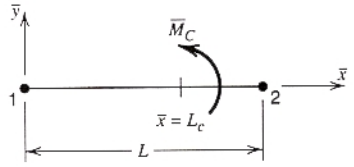

Figure P19.11

19.12. Derive the stiffness matrix in local coordinates for a *beam on elastic foundation* element. Use the shape functions described in Eq. (19.63b) and a Winkler model for the foundation. With the addition of the elastic foundation, the virtual work of the internal forces δU in the element is the virtual work due to beam bending plus the virtual work due to foundation deformation. That is,

$$\delta U = \int_0^L (\delta\bar{v})'' EI\bar{v}''\, d\bar{x} + \int_0^L \delta\bar{v} k\bar{v}\, d\bar{x}$$

where k is the foundation modulus [Eq. (10.3)].

REFERENCES

Works Cited in the Chapter

American Institute of Aeronautics and Astronautics (AIAA) (1985). *Proceedings Finite Element Standards Forum.* AIAA/ASME/ASCE/AHS 26th Structural Dynamics and Materials Conference, April 15, Orlando, Florida.

Boresi, A. P. and Chong, K. P. (2000). *Elasticity in Engineering Mechanics.* New York: Wiley

Clough, R. W. (1960). The Finite Element Method in Plane Stress Analysis. *Proceedings 2nd ASCE Conference on Electronic Computation.* Pittsburg, Pa. pp. 345–378.

Cook, R. D., Malkus, D. S., and Plesha, M. E. (1989). *Concepts and Applications of Finite Element Analysis*, 3rd ed. New York: Wiley.

Courant, R. (1950). *Differential and Integral Calculus.* New York: Wiley.

Courant, R. (1943). Variational Methods for the Solution of Problems of Equilibrium and Vibrations. *Bull. Amer. Math. Soc.*, **49**: 1–23.

Kellison, S. G. (1975). *Fundamentals of Numerical Analysis*, Homewood, Ill. Richard D. Irwin.

MacNeil, R. H. and Harder, R. L. (1984). A Proposed Standard Set of Problems to Test Finite Element Accuracy. *Proceedings AIAA/ASME/ASCE/AHS 25th Structural Dynamics and Materials Conference*, May 14, Palm Springs, Calif.

MacNeil, R. H. and Harder, R. L. (1985). A Proposed Standard Set of Problems to Test Finite Element Accuracy. *Finite Elements Anal. Des.* **1** (1). 3–20.

Turner, M. J., Clough, R. W., Martin, H. C., and Topp, L. J. (1956). Stiffness and Deflection Analysis of Complex Structures. *J. Aero. Sc.*, **25** (9): 805–823.

Zienkiewicz, O. C. and Taylor, R. L. (1989). *The Finite Element Method*, 4th ed. New York: McGraw-Hill.

Texts on the Finite Element Method

Baker, A. J. and Pepper, D. W. (1991). *Finite Elements 1-2-3.* New York: McGraw-Hill.

Bathe, K.-J. (1982). *Finite Element Procedures in Engineering Analysis.* Englewood Cliffs, N.J.: Prentice-Hall.

Bickford, W. B. (1990). *A First Course in the Finite Element Method.* Homewood, Ill.: Richard D. Irwin.

Burnett, D. S. (1987). *Finite Element Analysis, from Concepts to Applications.* Reading, Mass.: Addison-Wesley.

Cook, R. D., Malkus, D. S., and Plesha, M. E. (1989). *Concepts and Applications of Finite Element Analysis*, 3rd ed. New York: Wiley.

Crisfield, M. A. (1991). *Non-linear Finite Element Analysis of Solids and Structures.* New York: Wiley.

Ghali, A. and Neville, A. M. (1989). *Structural Analysis, A Unified Classical and Matrix Approach*, 3rd ed. London: Chapman and Hall.

Grandin, H., Jr. (1991). *Fundamentals of the Finite Element Method.* Prospect Heights, Ill.: Waveland Press.

Hughes, T. J. R. (1987). *The Finite Element Method, Linear Static and Dynamic Finite Element Analysis.* Englewood Cliffs, N.J.: Prentice-Hall.

Melosh, R. J. (1990). *Structural Engineering Analysis by Finite Elements.* Englewood Cliffs, N.J.: Prentice-Hall.

Potts, J. F. and Oler, J. W. (1989). *Finite Element Applications with Microcomputers.* Englewood Cliffs, N.J.: Prentice-Hall.

Przemieniecki, J.S. (1968). *Theory of Matrix Structural Analysis.* New York: McGraw-Hill.

Rao, S. S. (1989). *The Finite Element Method in Engineering*, 2nd ed. Oxford: Pergamon Press.

Reddy, J. N. (1984). *An Introduction to the Finite Element Method.* New York: McGraw-Hill.

Sack, R. L. (1989). *Matrix Structural Analysis.* Boston: PWS-Kent Publ. Co.

Stasa, F. L. (1985). *Applied Finite Element Analysis for Engineers.* New York: Holt, Rinehart and Winston.

Weaver, W., Jr. and Gere, J. M. (1990). *Matrix Analysis of Framed Structures*, 3rd ed. New York: Van Nostrand Reinhold.

Zienkiewicz, O. C. and Taylor, R. L. (1989). *The Finite Element Method*, 4th ed. New York: McGraw-Hill.